Path following control of planar snake robots using a cascaded approach

Pål Liljebäck, *Member, IEEE,* Idar U. Haugstuen, and Kristin Y. Pettersen, *Senior Member, IEEE*

***Abstract*—This paper considers path following control of snake robots along straight paths. Under the assumption that the forward velocity of the snake robot is nonzero and positive, we prove that the proposed path following controller $\mathcal{K}$-exponentially stabilizes a snake robot to any desired straight path. The performance of the path following controller is investigated through simulations and through experiments with a physical snake robot where the controller successfully steers the snake robot towards and along the desired straight path.**

***Index Terms*—Snake robot, Path following, Cascaded system, K-exponential stability.**

I. Introduction

INSPIRED by biological snake locomotion, snake robots carry the potential of meeting the growing need for robotic mobility in challenging environments. Snake robots consist of serially connected modules capable of bending in one or more planes. The many degrees of freedom of snake robots make them difficult to control, but provide traversability in irregular environments that surpasses the mobility of the more conventional wheeled, tracked and legged forms of robotic mobility.

This paper considers planar path following control of snake robots along straight paths. Straight line path following capabilities are important since they enable a snake robot to follow a desired path given by waypoints interconnected by straight lines. Straight line path following is therefore relevant for many future applications of snake robots, such as automated inspection rounds in inaccessible areas of industrial process facilities or mapping of confined spaces by moving along prescribed paths. Note that this paper considers path following, in contrast to trajectory tracking, where the goal is additionally to control the position of the system *along* the path. During path following, we steer the system towards and along the path, but do not consider the temporal position of the system along the path.

Research on snake locomotion has been conducted for several decades. Early research efforts on this topic include the work by Gray [1], who conducted empirical and analytical studies of snake locomotion already in the 1940s, and the work by Hirose [2], who studied biological snakes and developed mathematical relationships characterizing their motion. The emphasis in literature so far has mainly been on achieving forward and turning locomotion. For instance, the works in [3], [4] model the kinematics of a snake robot in terms of a continuous backbone curve and propose gaits for the backbone curve, such as a sidewinding gait. Sidewinding motion on slopes is considered in [5]. A variety of gaits for snake robots, including climbing gaits, are presented in [6]–[8]. The works in [9], [10] employ computer simulations to study properties of lateral undulation, which is the most common form of snake locomotion. [10] also proposes a forward velocity controller for snake robots. Control strategies for wheelless snake robots propelled by obstacle contact forces are proposed in [11], [12].

Previous research on not only achieving forward and turning locomotion, but also making a snake robot follow a desired path, is limited. A position and path following controller for a wheeled snake robot is proposed in [13], where also Lyapunov analysis is employed to analyze the controller. The work also considers approaches for preventing the snake robot from attaining a straight shape, which is singular with respect to propulsion. Similar approaches are presented in [14], [15], where a measure of dynamic manipulability that takes the constraint forces on the wheels into account is employed in order to control the position of the snake robot while simultaneously ensuring a high manipulability. The work in [16] considers trajectory tracking of snake robots where some, but not all, of the links are assumed to be wheeled. This gives the system more degrees of freedom and is utilized to follow a trajectory while simultaneously maintaining a high manipulability. Path following of a snake robot with active wheels is considered in [17], but no stability analysis of the controller is presented. The authors have previously employed *Poincaré maps* to study the stability properties of snake locomotion along a straight path [18]. The presented analysis is, however, based on numerical calculations and is thus only valid for a given set of controller parameters.

Research on robotic fish and eel-like mechanisms is relevant to research on snake robots since these mechanisms are very similar. The works in [19]–[21] synthesize gaits for translational and rotational motion of various fish-like mechanisms and propose controllers for tracking straight and curved trajectories. However, an analysis that formally proves that the fish-like mechanisms converge to the desired path still remains.

In this paper, we consider the problem of planar path following control of snake robots. As indicated by the above literature review, previous research on path following control of snake robots has focused on robots with nonholonomic constraints, i.e. where each link is constrained from moving sideways. In this paper, we consider snake robots where the links are allowed to slip sideways as we consider such snake robots to be more relevant to operations in unknown and cluttered environments, which represent the longterm goal of our research.

The contribution of this paper is a path following controller that enables snake robots to track planar straight paths. Using

Manuscript received June 28, 2010.

Affiliation of Pål Liljebäck is shared between the Dept. of Engineering Cybernetics at the Norwegian University of Science and Technology (NTNU), NO-7491 Trondheim, Norway, and SINTEF ICT, Dept. of Applied Cybernetics, N-7465 Trondheim, Norway. E-mail: Pal.Liljeback@sintef.no.

Idar U. Haugstuen and Kristin Y. Pettersen are with the Dept. of Engineering Cybernetics at the Norwegian University of Science and Technology (NTNU), NO-7491 Trondheim, Norway. E-mail: haugstue@stud.ntnu.no, Kristin.Y.Pettersen@itk.ntnu.no.

cascaded systems theory, we prove that the proposed path following controller $\mathcal{K}$-exponentially stabilizes a snake robot to any desired straight path. In particular, under the assumption that the forward velocity of the snake robot is nonzero and positive, we show that the model of the snake robot and the controller can be written as a cascaded system where the body shape changes affect the global orientation of the robot, which subsequently affects the cross-track error between the robot and the desired path. The $\mathcal{K}$-exponential stability of the cascaded system guarantees that the cross-track error and the heading of the snake robot with respect to the direction of the path converge to zero. To the authors' best knowledge, this is the first time the stability properties of a path following controller for a snake robot without nonholonomic constraints are formally proved. The performance of the path following controller is investigated through simulations and through experiments with a physical snake robot. The simulations and the experimental results show that the proposed controller successfully steers the snake robot towards and along the desired straight path.

Note that this paper is based on and extends preliminary work by the authors in [22], [23]. The extensions in this paper include new simulation results and new experimental results that better illustrate the performance of the proposed controller, inclusion of proofs of two lemmas that were omitted in [22], [23], and general improvements of the accuracy of important statements concerning the main result of the paper.

The paper is organized as follows. Section II presents some mathematical preliminaries. Section III presents the model of the snake robot. Section IV presents the path following controller. Simulation results and experimental results are presented in Section V and Section VI, respectively. Finally, Section VII presents some concluding remarks.

II. Mathematical preliminaries

We begin by presenting some stability concepts that will be employed in Section IV to analyse the straight line path following controller of the snake robot. The stability concepts make use of class $\mathcal{K}$ and class $\mathcal{KL}$ functions. A function being of class $\mathcal{K}$ basically means that the function is strictly increasing with respect to its argument. A function of class $\mathcal{KL}$ has two arguments, and is strictly increasing with respect to the first argument when the second argument is fixed, and is decreasing with respect to the second argument when the first argument is fixed. A formal definition of class $\mathcal{K}$ functions and class $\mathcal{KL}$ functions is given in [24] (Definition 4.2 and 4.3). Consider now the system

$$\dot{\boldsymbol{x}} = \boldsymbol{f}(t, \boldsymbol{x}), \tag{1}$$

where $f : \mathbb{R}_{\geq 0} \times \mathbb{R}^n \to \mathbb{R}^n$ is piecewise continuous in t and locally Lipschitz in $\boldsymbol{x}$.

Definition 1: (UGAS, see Lemma 4.5 in [24]).
The equilibrium point $\boldsymbol{x} = \boldsymbol{0}$ of the system (1) is uniformly globally asymptotically stable (UGAS) if there exists a class $\mathcal{KL}$ function β such that for any initial state $\boldsymbol{x}(t_0)$

$$\|\boldsymbol{x}(t)\| \leq \beta(\|\boldsymbol{x}(t_0)\|, t - t_0), \quad \forall t \geq t_0 \geq 0. \tag{2}$$

A system being UGAS basically means that the state $\boldsymbol{x}$ converges to zero as $t \to \infty$. A special case of UGAS arises when the class $\mathcal{KL}$ function β takes the form of an exponential function as follows.

Definition 2: (UGES, see Definition 4.5 in [24]).
The equilibrium point $\boldsymbol{x} = \boldsymbol{0}$ of the system (1) is uniformly globally exponentially stable (UGES) if there exist positive constants k and λ such that for any initial state $\boldsymbol{x}(t_0)$

$$\|\boldsymbol{x}(t)\| \leq k \|\boldsymbol{x}(t_0)\| e^{-\lambda(t-t_0)}, \quad \forall t \geq t_0 \geq 0. \tag{3}$$

A slightly weaker form of stability than exponential stability is $\mathcal{K}$-exponential stability, which is defined as follows.

Definition 3: (Global $\mathcal{K}$-exponential stability, see Definition 2 in [25]).
The equilibrium point $\boldsymbol{x} = \boldsymbol{0}$ of the system (1) is globally $\mathcal{K}$-exponentially stable if there exist a positive constant λ and a class $\mathcal{K}$ function α such that for any initial state $\boldsymbol{x}(t_0)$

$$\|\boldsymbol{x}(t)\| \leq \alpha(\|\boldsymbol{x}(t_0)\|) e^{-\lambda(t-t_0)}, \quad \forall t \geq t_0 \geq 0. \tag{4}$$

As first noted in [26], the following Corollary holds.

Corollary 4: Global $\mathcal{K}$-exponential stability is equivalent to the system being both UGAS and ULES (uniformly locally exponentially stable).

Remark 5: For simplicity, if the equilibrium point $\boldsymbol{x} = \boldsymbol{0}$ of a system is UGAS/UGES/globally $\mathcal{K}$-exponentially stable, we often say that the system itself is UGAS/UGES/globally $\mathcal{K}$-exponentially stable.

Next, consider the cascaded system

$$\dot{\boldsymbol{x}} = \boldsymbol{f}_1(t, \boldsymbol{x}) + \boldsymbol{g}(t, \boldsymbol{x}, \boldsymbol{y})\boldsymbol{y}, \tag{5}$$

$$\dot{\boldsymbol{y}} = \boldsymbol{f}_2(t, \boldsymbol{y}), \tag{6}$$

where $\boldsymbol{x} \in \mathbb{R}^n$, $\boldsymbol{y} \in \mathbb{R}^m$, $\boldsymbol{f}_1(t, \boldsymbol{x})$ is continuously differentiable in $(t, \boldsymbol{x})$, and $\boldsymbol{f}_2(t, \boldsymbol{y})$, $\boldsymbol{g}(t, \boldsymbol{x}, \boldsymbol{y})$ are continuous in their arguments and locally Lipschitz in $\boldsymbol{y}$ and $(\boldsymbol{x}, \boldsymbol{y})$, respectively. Many dynamical systems can be written in this cascaded form, where we see that the $\boldsymbol{y}$-dynamics in (6) perturbs the $\boldsymbol{x}$-dynamics in (5) through the interconnection term $\boldsymbol{g}(t, \boldsymbol{x}, \boldsymbol{y})\boldsymbol{y}$.

Theorem 6: (See Theorem 2 in [27]).
The cascaded system (5), (6) is UGAS if the following three assumptions are satisfied:
(A1) The system $\dot{\boldsymbol{x}} = \boldsymbol{f}_1(t, \boldsymbol{x})$ is UGAS with a radially unbounded Lyapunov function satisfying

$$\left\| \frac{\partial V}{\partial \boldsymbol{x}} \right\| \|\boldsymbol{x}\| \leq cV(t, \boldsymbol{x}), \quad \forall \|\boldsymbol{x}\| \geq \eta, \tag{7}$$

where $c > 0$ and $\eta > 0$ are constants.
(A2) The function $\boldsymbol{g}(t, \boldsymbol{x}, \boldsymbol{y})$ satisfies

$$\|\boldsymbol{g}(t, \boldsymbol{x}, \boldsymbol{y})\| \leq \theta_1(\|\boldsymbol{y}\|) + \theta_2(\|\boldsymbol{y}\|) \|\boldsymbol{x}\|, \tag{8}$$

where $\theta_1, \theta_2 : \mathbb{R}_{\geq 0} \to \mathbb{R}_{\geq 0}$ are continuous.
(A3) The system $\dot{\boldsymbol{y}} = \boldsymbol{f}_2(t, \boldsymbol{y})$ is UGAS and for all $t_0 \geq 0$

$$\int_{t_0}^{\infty} \|\boldsymbol{y}(t)\| \, dt \leq \kappa(\|\boldsymbol{y}(t_0)\|), \tag{9}$$

where the function $\kappa(\cdot)$ is a class $\mathcal{K}$ function.

Lemma 7: (See Lemma 8 in [28]).
If in addition to the assumptions in Theorem 6 both $\dot{\boldsymbol{x}} = \boldsymbol{f}_1(t, \boldsymbol{x})$ and $\dot{\boldsymbol{y}} = \boldsymbol{f}_2(t, \boldsymbol{y})$ are globally $\mathcal{K}$-exponentially stable, then the cascaded system (5), (6) is globally $\mathcal{K}$-exponentially stable.

III. The model of the snake robot

This section summarizes the model of the snake robot which the controller development in Section IV is based upon. For a more detailed presentation of the model, the reader is referred to [29].

TABLE I
THE PARAMETERS OF THE SNAKE ROBOT.

Symbol	Description
N	Number of links.
l	Length of a link.
m	Mass of a link.
$\boldsymbol{\phi} \in \mathbb{R}^{N-1}$	Joint coordinates.
$\theta \in \mathbb{R}$	Orientation of the robot.
$(p_x, p_y) \in \mathbb{R}^2$	CM position of the robot.
$\boldsymbol{v}_\phi \in \mathbb{R}^{N-1}$	Joint velocities.
$v_\theta \in \mathbb{R}$	Angular velocity of the robot.
$(v_t, v_n) \in \mathbb{R}^2$	Translational velocity of the robot.
$\boldsymbol{u} \in \mathbb{R}^{N-1}$	Joint actuator forces.

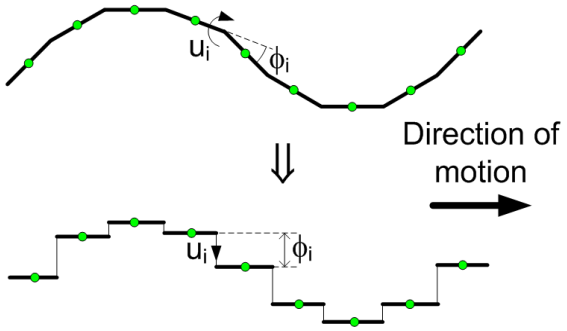

Fig. 1. The revolute joints of the snake robot are modelled as prismatic joints that displace the CM of each link transversal to the direction of motion.

A. Overview of the model

In this work, we employ a lumped parameter model to describe the dynamics of snake robots consisting of serially connected rigid links. Note that alternative modelling approaches also exist, such as continuum models, which assume that the snake robot can be described as a continuous curve [30]–[32]. The model formulation described in the following is based on a simplified modelling approach which is suitable for controller design purposes.

We consider a planar snake robot with links interconnected by active revolute joints. The surface beneath the robot is flat and horizontal, and each link is subjected to a viscous ground friction force. The body shape changes of the robot induce friction forces on the links that produce the translational and rotational motion of the robot. A simplified model that captures only the most essential part of the snake robot dynamics is proposed in [29]. The idea behind this model is illustrated in Fig. 1 and motivated by an analysis presented in [29], which shows that:

- The forward motion of a planar snake robot is produced by the link velocity components that are *normal* to the forward direction.
- The change in body shape during forward locomotion primarily consists of relative displacements of the CM of the links *normal* to the forward direction of motion.

Based on these two properties, the simplified model describes the body shape changes of a snake robot as *linear displacements* of the links with respect to each other instead of rotational displacements. The linear displacements occur *normal* to the forward direction of motion and produce friction forces that propel the robot forward. This essentially means that the revolute joints of the snake robot are modelled as prismatic (translational) joints and that the rotational motion of the links during body shape changes is disregarded. However, the model still captures the *effect* of the rotational link motion during body shape changes, which is a linear displacement of the CM of the links normal to the forward direction of motion. Note that the relative link displacements transversal to the direction of motion will *not* dominate over the relative link displacements tangential to the direction of motion when the amplitudes of the link angles become large. The simplified model is therefore a valid description of snake robot locomotion only as long as the link angles are limited.

The mathematical model of the snake robot is summarized in the next subsection in terms of the symbols illustrated in Fig. 2 and Fig. 3. The parameters of the snake robot are summarized in Table I.

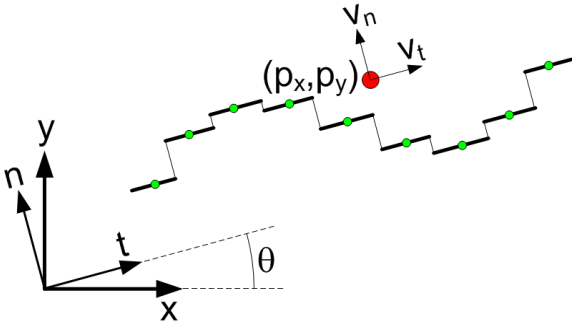

Fig. 2. Illustration of the two coordinate frames employed in the model. The global x-y frame is fixed. The t-n frame is always aligned with the snake robot.

B. Equations of motion

The snake robot has N links of length l and mass m interconnected by $N-1$ prismatic joints. The prismatic joints control the normal direction distance between the links. As seen in Fig. 3, the normal direction distance from link i to link $i+1$ is denoted by ϕ_i and represents the coordinate of joint i. The positive direction of ϕ_i is along the n axis.

The snake robot moves in the horizontal plane and has $N+2$ degrees of freedom. The motion is defined with respect to the two coordinate frames illustrated in Fig. 2. The x-y frame is the fixed global frame. The t-n frame is always aligned with the snake robot, i.e. the t and n axis always point in the *tangential* and *normal* direction of the robot, respectively. The origin of both frames are fixed and coincide.

As seen in Fig. 2, the global frame position of the CM

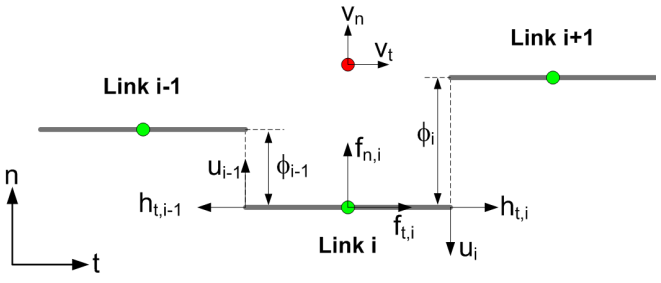

Fig. 3. Symbols characterizing the kinematics and dynamics of the snake robot.

(center of mass) of the snake robot is denoted by $(p_x, p_y) \in \mathbb{R}^2$. The global frame orientation, denoted by $\theta \in \mathbb{R}$, is defined as the angle between the t axis and the global x axis with counterclockwise positive direction.

Remark 8: A snake robot with revolute joints has no explicitly defined orientation since there is an independent link angle associated with each link. A common approach in previous literature has therefore been to describe the orientation of a snake robot as the mean of the absolute link angles [33], [34]. The simplified model employed in this paper avoids this issue since the scalar variable θ provides an explicit representation of the orientation of the snake robot, which is a significant advantage for control design purposes.

The state vector of the system is chosen as

$$\boldsymbol{x} = (\boldsymbol{\phi}, \theta, p_x, p_y, \boldsymbol{v}_\phi, v_\theta, v_t, v_n) \in \mathbb{R}^{2N+4}, \tag{10}$$

where $\boldsymbol{\phi} = (\phi_1, \cdots, \phi_{N-1}) \in \mathbb{R}^{N-1}$ are the joint coordinates, $\theta \in \mathbb{R}$ is the absolute orientation, $(p_x, p_y) \in \mathbb{R}^2$ is the global frame position of the CM, $\boldsymbol{v}_\phi = \dot{\boldsymbol{\phi}} \in \mathbb{R}^{N-1}$ are the joint velocities, $v_\theta = \dot{\theta} \in \mathbb{R}$ is the angular velocity, and $(v_t, v_n) \in \mathbb{R}^2$ is the tangential and normal direction velocity of the snake robot. Note that we define the position with respect to the global frame, but the translational velocity with respect to the t-n frame.

As illustrated in Fig. 3, each link is influenced by a ground friction force (acting on the CM of the link) and constraint forces that hold the joints together. A model of these forces is presented in [29], where it is also shown that the complete model of the snake robot can be written as

$$\dot{\boldsymbol{\phi}} = \boldsymbol{v}_\phi, \tag{11a}$$
$$\dot{\theta} = v_\theta, \tag{11b}$$
$$\dot{p}_x = v_t \cos\theta - v_n \sin\theta, \tag{11c}$$
$$\dot{p}_y = v_t \sin\theta + v_n \cos\theta \tag{11d}$$
$$\dot{\boldsymbol{v}}_\phi = -\frac{c_1}{m}\boldsymbol{v}_\phi + \frac{c_2}{m} v_t \boldsymbol{A}\boldsymbol{D}^T\boldsymbol{\phi} + \frac{1}{m}\boldsymbol{D}\boldsymbol{D}^T\boldsymbol{u}, \tag{11e}$$
$$\dot{v}_\theta = -c_3 v_\theta + \frac{c_4}{N-1} v_t \overline{\boldsymbol{e}}^T\boldsymbol{\phi}, \tag{11f}$$
$$\dot{v}_t = -\frac{c_1}{m} v_t + \frac{2c_2}{Nm} v_n \overline{\boldsymbol{e}}^T\boldsymbol{\phi} - \frac{c_2}{Nm}\boldsymbol{\phi}^T\boldsymbol{A}\overline{\boldsymbol{D}}\boldsymbol{v}_\phi, \tag{11g}$$
$$\dot{v}_n = -\frac{c_1}{m} v_n + \frac{2c_2}{Nm} v_t \overline{\boldsymbol{e}}^T\boldsymbol{\phi}, \tag{11h}$$

where $\boldsymbol{u} \in \mathbb{R}^{N-1}$ are the actuator forces at the joints and

$\overline{\boldsymbol{e}} = \begin{bmatrix} 1 & . & . & 1 \end{bmatrix}^T \in \mathbb{R}^{N-1}$,

$\overline{\boldsymbol{D}} = \boldsymbol{D}^T\left(\boldsymbol{D}\boldsymbol{D}^T\right)^{-1} \in \mathbb{R}^{N\times(N-1)}$,

$$\boldsymbol{A} = \begin{bmatrix} 1 & 1 & & \\ & . & . & \\ & & . & . \\ & & & 1 \quad 1 \end{bmatrix}, \boldsymbol{D} = \begin{bmatrix} 1 & -1 & & \\ & . & . & \\ & & . & . \\ & & & 1 \quad -1 \end{bmatrix},$$

and where $\boldsymbol{A} \in \mathbb{R}^{(N-1)\times N}$ and $\boldsymbol{D} \in \mathbb{R}^{(N-1)\times N}$. The parameters c_1, c_2, c_3, and c_4 are positive scalar friction coefficients that characterize the external forces acting on the snake robot. In particular, the coefficient c_1 determines the magnitude of the friction forces resisting the link motion, c_2 determines the magnitude of the induced friction forces that propel the snake robot forward, c_3 determines the friction torque opposing the rotation of the snake robot, while c_4 determines the induced torque that rotates the snake robot. This torque is induced when the forward direction velocity and the average of the joint coordinates are nonzero. The role of each coefficient is explained in more detail in [29].

IV. Design and analysis of the path following controller

In this section, we design and analyse a straight line path following controller for the snake robot.

A. Control objective

The control objective is to steer the snake robot so that it converges to and subsequently tracks a straight path while maintaining a heading which is parallel to the path. To this end, we define the global coordinate system so that the global x axis is aligned with the desired straight path. The position of the snake robot along the global y axis, p_y, is therefore the shortest distance from the robot to the desired path and the orientation of the snake robot, θ, is the angle that the robot forms with the desired path. The control objective is thus to regulate p_y and θ to zero. Since snake robot locomotion is a slow form of robotic mobility which is generally employed for traversability purposes, the authors consider it less important to accurately control the forward velocity of the robot. During path following with a snake robot, it therefore makes sense to focus all the control efforts on converging to the path and subsequently progressing along the path at some nonzero forward velocity $v_t \in [V_{\min}, V_{\max}]$, where $V_{\min}$ and $V_{\max}$ represent the boundaries of some positive interval in which we would like the forward velocity to be contained.

From the above discussion, the control problem is to design a feedback control law

$$\boldsymbol{u} = \boldsymbol{u}(t, \boldsymbol{\phi}, \theta, p_y, \boldsymbol{v}_\phi, v_\theta, v_t, v_n) \in \mathbb{R}^{N-1} \tag{12}$$

such that the following control objectives are reached:

$$\lim_{t\to\infty} p_y(t) = 0, \tag{13}$$
$$\lim_{t\to\infty} \theta(t) = 0. \tag{14}$$

B. Assumptions

A planar snake robot achieves forward motion through periodic body shape changes that generate external forces on the robot from the environment which propel the robot forward. The most common form of such periodic body shape changes is called *lateral undulation* [2] and consists of horizontal waves that are propagated backwards along the snake body from head to tail. The work by the authors in [35], which investigates the velocity dynamics of a snake robot during lateral undulation, shows that the forward velocity during lateral undulation oscillates around a positive nonzero average velocity that can be predetermined based on the parameters characterizing the gait pattern. In other words, when the snake robot conducts lateral undulation, the results in [35] suggest that the forward velocity is contained in some nonzero and positive interval $[V_{\min}, V_{\max}]$ that can be scaled based on a set of gait pattern parameters. We therefore choose to base the path following controller of the snake robot on the following assumption:

Assumption 9: The snake robot conducts *lateral undulation* and has a forward velocity which is always nonzero and positive, i.e. $v_t \in [V_{\min}, V_{\max}]\ \forall\ t \geq 0$ where $V_{\max} \geq V_{\min} > 0$.

Remark 10: The validity of Assumption 9 can be seen by inspecting the equations of motion in (11). The dynamics of the forward velocity in (11g) contains three terms. As shown in [35], the term $-\frac{c_2}{Nm}\boldsymbol{\phi}^T\boldsymbol{A}\overline{\boldsymbol{D}}\boldsymbol{v}_\phi$ is positive and accelerates the robot forward during lateral undulation, while the term $-\frac{c_1}{m}v_t$ is the ground friction force. The combined effect of these two terms can never make the forward velocity v_t become zero during lateral undulation. This leaves $\frac{2c_2}{Nm}v_n\overline{\boldsymbol{e}}^T\boldsymbol{\phi}$ as the only term that can produce a negative forward acceleration that forces v_t to zero. This term is negative when the sideways velocity v_n and the sum of the joint coordinates $\overline{\boldsymbol{e}}^T\boldsymbol{\phi}$ have opposite signs. However, it can be seen from (11h) that v_n and $\overline{\boldsymbol{e}}^T\boldsymbol{\phi}$ will always tend in the same rather than the opposite direction when $v_t > 0$. It is therefore unlikely for v_n and $\overline{\boldsymbol{e}}^T\boldsymbol{\phi}$ to have opposite signs over the long period required to force v_t to zero.

C. Model transformation

On the basis of the discussion above and Assumption 9, we will not control the dynamics of the forward velocity v_t given by (11g) and instead treat the forward velocity as a positive parameter satisfying $v_t \in [V_{\min}, V_{\max}]$.

As seen in (11f) and (11h), the joint coordinates $\boldsymbol{\phi}$ are present in the dynamics of both the angular velocity v_θ and the sideways velocity v_n of the snake robot. This complicates the controller design since the body shape changes will affect both the heading and the sideways motion of the robot. Motivated by [36], we see that it is possible to remove the effect of $\boldsymbol{\phi}$ on the sideways velocity by a coordinate transformation. In particular, we move the point that determines the position of the snake robot a distance ϵ along the tangential direction of the robot from the CM to a new location, which is precisely where the body shape changes of the robot (characterized by $\overline{\boldsymbol{e}}^T\boldsymbol{\phi}$) generate a pure rotational motion and no sideways force. This coordinate transformation is illustrated to the left in Fig. 4 and is defined as

$$\overline{p}_x = p_x + \epsilon\cos\theta, \tag{15a}$$
$$\overline{p}_y = p_y + \epsilon\sin\theta, \tag{15b}$$
$$\overline{v}_n = v_n + \epsilon v_\theta, \tag{15c}$$

where ϵ is a constant parameter defined as

$$\epsilon = -\frac{2\,(N-1)}{Nm}\frac{c_2}{c_4}. \tag{16}$$

With the new coordinates in (15), the model (11) is transformed into

$$\dot{\boldsymbol{\phi}} = \boldsymbol{v}_\phi, \tag{17a}$$
$$\dot{\theta} = v_\theta, \tag{17b}$$
$$\dot{\overline{p}}_y = v_t\sin\theta + \overline{v}_n\cos\theta, \tag{17c}$$
$$\dot{\boldsymbol{v}}_\phi = -\frac{c_1}{m}\boldsymbol{v}_\phi + \frac{c_2}{m}v_t\boldsymbol{A}\boldsymbol{D}^T\boldsymbol{\phi} + \frac{1}{m}\boldsymbol{D}\boldsymbol{D}^T\boldsymbol{u}, \tag{17d}$$
$$\dot{v}_\theta = -c_3 v_\theta + \frac{c_4}{N-1}v_t\overline{\boldsymbol{e}}^T\boldsymbol{\phi}, \tag{17e}$$
$$\dot{\overline{v}}_n = Xv_\theta + Y\overline{v}_n, \tag{17f}$$

where, by Assumption 9, the parameter $v_t \in [V_{\min}, V_{\max}]$ with $V_{\max} \geq V_{\min} > 0$, and where

$$X = \epsilon\left(\frac{c_1}{m} - c_3\right), \tag{18a}$$
$$Y = -\frac{c_1}{m}. \tag{18b}$$

The two scalar constants X and Y have been introduced in (17f) for simplicity of notation in the following sections. Note also that (11c) is not included in (17) since we do not consider the temporal position of the system along the path during path following.

D. The path following controller

The path following controller of the snake robot consists of two main components. The first component is the gait pattern controller, which propels the snake robot forward according to the gait pattern *lateral undulation* (as stated in Assumption 9). The second component is the heading controller, which steers the snake robot towards and subsequently along the desired path. The two components of the path following controller are now presented.

1) Gait pattern controller: As proposed in [2], lateral undulation is achieved by controlling joint $i \in \{1, \cdots, N-1\}$ of the snake robot according to the sinusoidal reference

$$\phi_{i,\text{ref}} = \alpha\sin\left(\omega t + (i-1)\,\delta\right) + \phi_o, \tag{19}$$

where α and ω are the amplitude and frequency, respectively, of the sinusoidal joint motion and δ determines the phase shift between the joints. The parameter ϕ_o is a joint offset coordinate that the heading controller will use to control the direction of the locomotion. As shown in [37], the average forward velocity v_t^* of the snake robot during straight path motion is given by

$$v_t^* = \frac{c_2}{2Nc_1}\alpha^2\omega k_\delta, \tag{20}$$

where k_δ is a constant parameter determined by the phase shift δ. This relation can be used to choose the gait parameters α, ω, and δ in order to achieve the desired average forward velocity.

In order to make the joints track the joint reference coordinates given by (19), we set the actuator forces according to the linearizing control law

$$\boldsymbol{u} = m\left(\boldsymbol{D}\boldsymbol{D}^T\right)^{-1}\left(\overline{\boldsymbol{u}} + \frac{c_1}{m}\dot{\boldsymbol{\phi}} - \frac{c_2}{m}v_t\boldsymbol{A}\boldsymbol{D}^T\boldsymbol{\phi}\right), \tag{21}$$

where $\overline{\boldsymbol{u}} \in \mathbb{R}^{N-1}$ is a new set of control inputs. This control law transforms the joint dynamics (17d) into $\dot{\boldsymbol{v}}_\phi = \ddot{\boldsymbol{\phi}} = \overline{\boldsymbol{u}}$. Subsequently, we choose the new control input $\overline{\boldsymbol{u}}$ as

$$\overline{\boldsymbol{u}} = \ddot{\boldsymbol{\phi}}_{\text{ref}} + k_{v_\phi}\left(\dot{\boldsymbol{\phi}}_{\text{ref}} - \dot{\boldsymbol{\phi}}\right) + k_\phi\left(\boldsymbol{\phi}_{\text{ref}} - \boldsymbol{\phi}\right), \tag{22}$$

where $k_\phi > 0$ and $k_{v_\phi} > 0$ are scalar controller gains and $\boldsymbol{\phi}_{\text{ref}} = (\phi_{1,\text{ref}}, \cdots, \phi_{N-1,\text{ref}}) \in \mathbb{R}^{N-1}$ are the joint reference coordinates given by (19). By introducing the error variable

$$\widetilde{\boldsymbol{\phi}} = \boldsymbol{\phi} - \boldsymbol{\phi}_{\text{ref}}, \tag{23}$$

the joint dynamics given by (17a) and (17d) can be written in terms of the error dynamics

$$\ddot{\widetilde{\boldsymbol{\phi}}} + k_{v_\phi}\dot{\widetilde{\boldsymbol{\phi}}} + k_\phi\widetilde{\boldsymbol{\phi}} = \boldsymbol{0}, \tag{24}$$

which is clearly *exponentially stable* [24] as long as $\boldsymbol{\phi}_{\text{ref}}$, $\dot{\boldsymbol{\phi}}_{\text{ref}}$, and $\ddot{\boldsymbol{\phi}}_{\text{ref}}$ are bounded. This means that the joint coordinates exponentially track the reference coordinates given by (19).

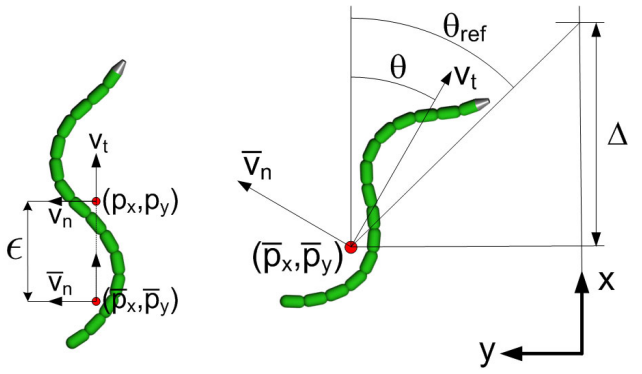

Fig. 4. Left: The coordinate transformation of the snake robot. Right: The Line-of-Sight (LOS) guidance law.

2) Heading controller: In order to steer the snake robot towards the desired straight path, we employ the Line-of-Sight (LOS) guidance law

$$\theta_{\text{ref}} = -\arctan(\frac{\overline{p}_y}{\Delta}), \tag{25}$$

where $\overline{p}_y$ is the cross-track error and $\Delta > 0$ is a design parameter referred to as the *look-ahead distance*. This LOS guidance law is commonly used during e.g. path following control of marine surface vessels [38], [39]. As illustrated to the right in Fig. 4, the LOS angle θ_{ref} corresponds to the orientation of the snake robot when it is headed towards the point located a distance Δ ahead of the snake robot along the desired path. The value of Δ is important since it determines the rate of convergence to the desired path.

As mentioned in Section IV-D1, we will use the joint offset coordinate ϕ_o in (19) to ensure that the heading of the snake robot θ tracks the LOS angle given by (25). Motivated by [39] and [40], we conjecture that making θ track the LOS angle θ_{ref} will make the snake converge to the desired path and subsequently follow the path with its heading parallel to the path. In other words, we conjecture that a control law making θ track θ_{ref} will fulfill the control objectives (13) and (14). To derive the control law for ϕ_o, we first rewrite the dynamics of v_θ given by (17e) with the new coordinates $\widetilde{\boldsymbol{\phi}}$ in (23), which gives the dynamics of v_θ as a function of the joint reference coordinates given by (19). From (23), we have that $\boldsymbol{\phi} = \boldsymbol{\phi}_{\text{ref}} + \widetilde{\boldsymbol{\phi}}$. Using (19), we can therefore rewrite (17e) as

$$\begin{aligned} \dot{v}_\theta &= -c_3 v_\theta + c_4 v_t \phi_o \\ &+ \tfrac{c_4}{N-1} v_t \left(\sum_{i=1}^{N-1} \alpha \sin(\omega t + (i-1)\,\delta) + \overline{\boldsymbol{e}}^T \widetilde{\boldsymbol{\phi}} \right). \end{aligned} \tag{26}$$

Consequently, choosing ϕ_o as

$$\begin{aligned} \phi_o = \tfrac{1}{c_4 v_t} \Big(&\ddot{\theta}_{\text{ref}} + c_3 \dot{\theta}_{\text{ref}} - k_\theta(\theta - \theta_{\text{ref}}) \\ &- \tfrac{c_4}{N-1} v_t \sum_{i=1}^{N-1} \alpha \sin(\omega t + (i-1)\,\delta) \Big), \end{aligned} \tag{27}$$

where $k_\theta > 0$ is a scalar controller gain, enables us to write the dynamics of the heading angle θ, which is given by (17b) and (17e), in terms of the error dynamics

$$\ddot{\widetilde{\theta}} + c_3 \dot{\widetilde{\theta}} + k_\theta \widetilde{\theta} = \frac{c_4}{N-1} v_t \overline{\boldsymbol{e}}^T \widetilde{\boldsymbol{\phi}}, \tag{28}$$

where we have introduced the error variable

$$\widetilde{\theta} = \theta - \theta_{\text{ref}}. \tag{29}$$

Remark 11: The joint coordinate offset in (27) depends on the inverse of the forward velocity v_t. This does not represent a problem since, by Assumption 9, the forward velocity is always nonzero. When implementing the path following controller, this issue can be avoided by activating the controller *after* the snake robot has obtained a positive forward velocity.

Remark 12: The error dynamics of the joints in (24) and the error dynamics of the heading in (28) represent a cascaded system. In particular, the system (24) perturbs the system (28) through the interconnection term $\frac{c_4}{N-1} v_t \overline{\boldsymbol{e}}^T \widetilde{\boldsymbol{\phi}}$. Using cascaded systems theory, it will be shown in Section IV-F that the origin of this cascaded system is globally $\mathcal{K}$-exponentially stable.

We have now presented the complete path following controller of the snake robot. The structure of the complete controller is summarized in Fig. 5.

E. Main result

Based on the guidance and control laws presented in the previous subsection, we now formulate the main result of this paper. The result specifies a lower bound on the look-ahead distance Δ employed in (25). The bound on Δ, which is formally derived in the proof presented in Section IV-F, is given a physical interpretation in Remark 15 below.

Theorem 13: Consider a planar snake robot described by the model (17) and suppose that Assumption 9 is satisfied. If the look-ahead distance Δ of the LOS guidance law (25) is chosen such that

$$\Delta > \frac{|X|}{|Y|} \left(1 + \frac{V_{\max}}{V_{\min}} \right), \tag{30}$$

then the path following controller defined by (19), (21), (22), (25), and (27) guarantees that the control objectives (13) and (14) are achieved for any set of initial conditions satisfying $v_t \in [V_{\min}, V_{\max}]$.

Proof: The proof of this theorem is given in Section IV-F. ■

Remark 14: Theorem 13 does not specify the boundary values $V_{\min}$ and $V_{\max}$ of the interval in which the forward velocity v_t is contained. By Assumption 9, however, there exists a positive interval that contains v_t for all time $t \geq 0$. In practice, conservative values for these boundary values can be chosen, but in order to achieve a tighter bound on Δ, we would like to specify $V_{\min}$ and $V_{\max}$ as a function of the gait pattern parameters α, ω, δ, and ϕ_o. This remains a topic of future work.

Remark 15: The lower bound on the look-ahead distance Δ in (30) ensures that the sideways velocity $\overline{v}_n$ of the snake robot in (17f) is well behaved under the perturbations from the angular velocity v_θ. In particular, the magnitude of v_θ during convergence to the desired path is determined by the look-ahead distance Δ, i.e. the robot rotates fast when Δ is small (and vice versa). We see from (17f) that v_θ only has a small influence on $\overline{v}_n$ when $|X| \ll |Y|$, which means that we then can allow the magnitude of v_θ to be large, i.e. Δ can be small. Similarly, v_θ has a great influence on $\overline{v}_n$ when $|X| \gg |Y|$, which means that the magnitude of v_θ must be restricted, i.e. Δ must be large. These conditions are directly reflected by the lower bound in (30).

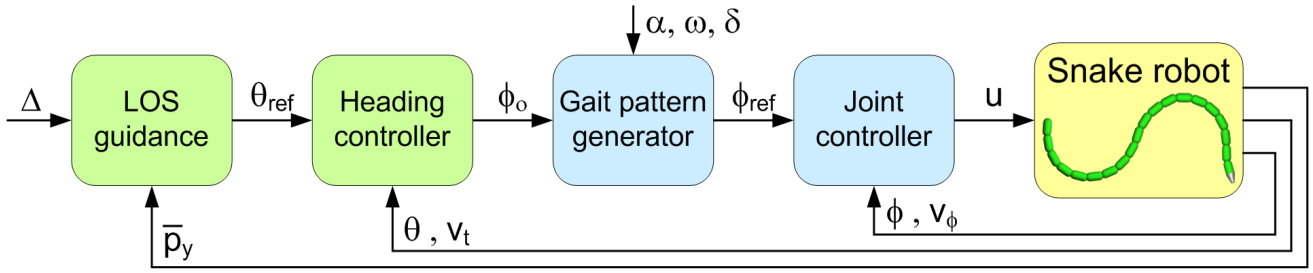

Fig. 5. The structure of the path following controller.

Remark 16: As explained in Section III-A, the assumptions underlying the simplified model are only valid as long as the link angles with respect to the forward direction are limited. The stability result in Theorem 13 is therefore claimed only for snake robots conducting lateral undulation with limited link angles.

F. Proof of the main result

We will prove Theorem 13 in three steps. In the first step, we show that the complete system, including the path following controller, can be written as a cascaded system. In the second step, we prove stability of the nominal systems in the cascade. Finally, we derive bounds on the interconnection terms between the nominal systems, which, by Theorem 6 and Lemma 7, allow us to conclude stability of the complete cascaded system. We will follow the steps of a similar proof presented in [41].

We begin by rewriting the dynamics of the cross-track error $\overline{p}_y$ and the sideways velocity $\overline{v}_n$ in terms of the heading error $\widetilde{\theta}$. From (29) and (25) we have that

$$\theta = -\arctan(\frac{\overline{p}_y}{\Delta}) + \widetilde{\theta}. \tag{31}$$

By using the relations $\sin(-\arctan(\frac{\overline{p}_y}{\Delta})) = -\frac{\overline{p}_y}{\sqrt{\overline{p}_y^2+\Delta^2}}$ and $\cos(-\arctan(\frac{\overline{p}_y}{\Delta})) = \frac{\Delta}{\sqrt{\overline{p}_y^2+\Delta^2}}$, it can be verified that (17c) can be written in terms of the heading error $\widetilde{\theta}$ as

$$\dot{\overline{p}}_y = -\frac{v_t}{\sigma}\overline{p}_y + \frac{\Delta}{\sigma}\overline{v}_n + \gamma\widetilde{\theta}, \tag{32}$$

where

$$\sigma = \sqrt{\overline{p}_y^2 + \Delta^2}, \tag{33}$$

$$\gamma = \frac{\sin\widetilde{\theta}}{\widetilde{\theta}}\frac{\left(v_t\Delta + \overline{v}_n\overline{p}_y\right)}{\sigma} + \frac{1-\cos\widetilde{\theta}}{\widetilde{\theta}}\frac{\left(v_t\overline{p}_y - \overline{v}_n\Delta\right)}{\sigma}. \tag{34}$$

Through similar manipulations, we can rewrite (17f) in the new coordinates as

$$\dot{\overline{v}}_n = \frac{X\Delta v_t}{\sigma^3}\overline{p}_y + \left(Y - \frac{X\Delta^2}{\sigma^3}\right)\overline{v}_n - \frac{X\Delta}{\sigma^2}\gamma\widetilde{\theta} + X\dot{\widetilde{\theta}}. \tag{35}$$

Collecting the error variables as

$$\boldsymbol{\eta} = \begin{bmatrix}\widetilde{\boldsymbol{\phi}} \\ \dot{\widetilde{\boldsymbol{\phi}}}\end{bmatrix} \in \mathbb{R}^{2N-2}, \quad \boldsymbol{\xi} = \begin{bmatrix}\widetilde{\theta} \\ \dot{\widetilde{\theta}}\end{bmatrix} \in \mathbb{R}^2, \tag{36}$$

and using (24), (28), (32), and (35), the model of the snake robot (17) during path following can be written as

$$\begin{bmatrix}\dot{\overline{p}}_y \\ \dot{\overline{v}}_n\end{bmatrix} = \boldsymbol{C}(\overline{p}_y)\begin{bmatrix}\overline{p}_y \\ \overline{v}_n\end{bmatrix} + \boldsymbol{H}_\xi(\overline{p}_y, \overline{v}_n, \boldsymbol{\xi})\boldsymbol{\xi}, \tag{37a}$$

$$\dot{\boldsymbol{\xi}} = \begin{bmatrix}0 & 1 \\ -k_\theta & -c_3\end{bmatrix}\boldsymbol{\xi} + \boldsymbol{H}_\eta\boldsymbol{\eta}, \tag{37b}$$

$$\dot{\boldsymbol{\eta}} = \begin{bmatrix}\boldsymbol{0} & \boldsymbol{I} \\ -k_\phi\boldsymbol{I} & -k_{v_\phi}\boldsymbol{I}\end{bmatrix}\boldsymbol{\eta}, \tag{37c}$$

where $\boldsymbol{I} \in \mathbb{R}^{(N-1)\times(N-1)}$ is the identity matrix and

$$\boldsymbol{H}_\eta = \begin{bmatrix}\boldsymbol{0} & \boldsymbol{0} \\ \frac{c_4}{N-1}v_t\overline{\boldsymbol{e}}^T & \boldsymbol{0}\end{bmatrix}, \tag{38}$$

$$\boldsymbol{H}_\xi(\overline{p}_y, \overline{v}_n, \boldsymbol{\xi}) = \begin{bmatrix}\gamma & 0 \\ -\frac{X\Delta}{\sigma^2}\gamma & X\end{bmatrix}, \tag{39}$$

$$\boldsymbol{C}(\overline{p}_y) = \begin{bmatrix}-\frac{v_t}{\sigma} & \frac{\Delta}{\sigma} \\ \frac{X\Delta v_t}{\sigma^3} & \left(Y - \frac{X\Delta^2}{\sigma^3}\right)\end{bmatrix}. \tag{40}$$

The system (37) is a cascaded system. In particular, the $\boldsymbol{\eta}$-dynamics in (37c) perturbs the $\boldsymbol{\xi}$-dynamics in (37b) through the interconnection term $\boldsymbol{H}_\eta\boldsymbol{\eta}$, and the $\boldsymbol{\xi}$-dynamics perturbs the $(\overline{p}_y, \overline{v}_n)$-dynamics in (37a) through the interconnection term $\boldsymbol{H}_\xi(\overline{p}_y, \overline{v}_n, \boldsymbol{\xi})\boldsymbol{\xi}$.

We now investigate the stability of the nominal systems of the cascade, i.e. all parts of (37) except the interconnection terms. The origin $\boldsymbol{\eta} = \boldsymbol{0}$ of the linear system (37c) and the origin $\boldsymbol{\xi} = \boldsymbol{0}$ of the linear nominal system in (37b) are globally exponentially stable (see Definition 4.5 in [24]) since the system matrices clearly are Hurwitz for k_θ, c_3, k_ϕ, $k_{v_\phi} > 0$. The nominal system of (37a) is given by

$$\begin{bmatrix}\dot{\overline{p}}_y \\ \dot{\overline{v}}_n\end{bmatrix} = \boldsymbol{C}(\overline{p}_y)\begin{bmatrix}\overline{p}_y \\ \overline{v}_n\end{bmatrix} \tag{41}$$

and has the stability properties established by the following two Lemmas.

Lemma 17: Under the conditions of Theorem 13, the origin of the system (41) is UGAS with a quadratic Lyapunov function.

Proof: The proof of this Lemma has previously been presented in [41] and is included in Appendix A for completeness. ■

Lemma 18: Under the conditions of Theorem 13, the origin of the system (41) is globally $\mathcal{K}$-exponentially stable.

Proof: The proof of this Lemma is presented in Appendix B. ■

Since exponential stability implies $\mathcal{K}$-exponential stability, we can conclude that all nominal systems of the cascade (37)

are globally $\mathcal{K}$-exponentially stable. Next, we derive bounds on the interconnection terms in the cascade. The induced 2-norm of the matrix $\boldsymbol{H}_\eta$ satisfies (see Appendix A in [24])

$$\|\boldsymbol{H}_\eta\|_2 \leq \sqrt{2N-2}\max_j \sum_{i=1}^{2}\{\boldsymbol{H}_\eta\}_{ij} \leq \frac{\sqrt{2}c_4 V_{\max}}{\sqrt{N-1}}, \quad (42)$$

while the induced 2-norm of the matrix $\boldsymbol{H}_\xi(\overline{p}_y, \overline{v}_n, \boldsymbol{\xi})$ satisfies

$$\begin{aligned}\|\boldsymbol{H}_\xi\|_2 &\leq \sqrt{2}\max_j \textstyle\sum_{i=1}^{2}\{\boldsymbol{H}_\xi\}_{ij} \\ &\leq \sqrt{2}\max\left(|\gamma| + \tfrac{|X|\Delta}{\sigma^2}|\gamma|, |X|\right) \\ &\leq \sqrt{2}\left(|\gamma| + \tfrac{|X|\Delta}{\sigma^2}|\gamma| + |X|\right).\end{aligned} \quad (43)$$

The function γ given by (34) is bounded according to

$$\begin{aligned}\gamma &\leq \left|\tfrac{\sin\tilde{\theta}}{\tilde{\theta}}\right|\tfrac{V_{\max}\Delta + |\overline{v}_n||\overline{p}_y|}{\sigma} + \left|\tfrac{1-\cos\tilde{\theta}}{\tilde{\theta}}\right|\tfrac{V_{\max}|\overline{p}_y| + |\overline{v}_n|\Delta}{\sigma} \\ &\leq \tfrac{V_{\max}\Delta}{\sigma} + \tfrac{|\overline{v}_n||\overline{p}_y|}{\sigma} + \tfrac{V_{\max}|\overline{p}_y|}{\sigma} + \tfrac{|\overline{v}_n|\Delta}{\sigma} \\ &\leq 2V_{\max} + 2|\overline{v}_n|.\end{aligned} \quad (44)$$

By inserting (44) into (43), it is straightforward to verify that

$$\|\boldsymbol{H}_\xi\|_2 \leq \mathcal{F}_1 + \mathcal{F}_2 \left\| \begin{bmatrix} \overline{p}_y \\ \overline{v}_n \end{bmatrix} \right\|_2, \quad (45)$$

where

$$\mathcal{F}_1 = \sqrt{2}\left(2V_{\max}\left(1 + \frac{|X|}{\Delta}\right) + |X|\right), \quad (46)$$

$$\mathcal{F}_2 = 2\sqrt{2}\left(1 + \frac{|X|}{\Delta}\right). \quad (47)$$

We are now ready to apply Theorem 6 to the cascaded system (37). We first consider the cascade of (37b) and (37c), for which it is straightforward to verify that Assumptions A1 and A3 of Theorem 6 are satisfied since the system (37c) and the nominal system of (37b) are both *globally exponentially stable*. Furthermore, Assumption A2 is trivially satisfied since $\|\boldsymbol{H}_\eta\|_2$ is bounded by the constant derived in (42). The cascaded system (37b), (37c) is therefore UGAS and, by Lemma 7, also globally $\mathcal{K}$-exponentially stable.

Next, we consider the cascade of (37a) and (37b), for which Assumption A1 of Theorem 6 is satisfied since, by Lemma 17, the nominal system of (37a) is UGAS with a quadratic Lyapunov function. Furthermore, it follows directly from (45) that Assumption A2 is satisfied. Finally, since the perturbing system (37b) is globally $\mathcal{K}$-exponentially stable, Assumption A3 is satisfied since the bound in Assumption A3 is easily shown to hold for any $\mathcal{K}$-exponentially stable system by integrating both sides of (4) from t_0 to ∞. The cascaded system (37a), (37b) is therefore UGAS and, by Lemma 7, also globally $\mathcal{K}$-exponentially stable since the nominal system of (37a) and the perturbing system (37b) are both globally $\mathcal{K}$-exponentially stable.

In summary, the complete cascaded system (37) is globally $\mathcal{K}$-exponentially stable. This means that $\overline{p}_y(t) \to 0$ and $\widetilde{\theta}(t) \to 0$, which, by (31), implies that $\theta(t) \to 0$, which means that control objective (14) is achieved. It subsequently follows from (15b) that $p_y(t) \to 0$, which means that control objective (13) is achieved. This completes the proof of Theorem 13.

Remark 19: Any gait pattern controller that exponentially stabilizes the error variable (23), i.e. not just the joint controller proposed in (21) and (22), makes the complete cascaded system globally $\mathcal{K}$-exponentially stable. This is a nice feature of cascaded systems theory.

V. Simulation study

In this section, we present simulation results that illustrate the performance of the proposed path following controller.

A. Simulation Parameters

The model of the snake robot (11) and the path following controller defined by (19), (21), (22), (25), and (27) were implemented and simulated in *Matlab R2008b* on a laptop running *Windows XP*. The model dynamics was calculated using the *ode45* solver in Matlab with a relative and absolute error tolerance of 10^{-6}.

We considered a snake robot with $N = 10$ links of length $l = 0.14$ m and mass $m = 1$ kg. Furthermore, we chose the friction coefficients as $c_1 = 0.45$, $c_2 = 3$, $c_3 = 0.5$ and $c_4 = 20$, the controller gains as $k_\phi = 20$, $k_{v_\phi} = 5$, and $k_\theta = 0.05$, and calculated the coordinate transformation distance according to (16) as $\epsilon = -27$ cm. The gait parameters were $\alpha = 0.1$ m, $\omega = 70°$/s, and $\delta = 40°$, which by (20) corresponds to the average forward velocity $v_t^* = \frac{c_2}{2Nc_1}\alpha^2\omega k_\delta = 0.1$ m/s. By making the conjecture that the forward velocity will always be contained in the interval $v_t \in [V_{\min}, V_{\max}] = [0.5v_t^*, 2v_t^*] = [0.05 \text{ m/s}, 0.2 \text{ m/s}]$, the lower bound on the look-ahead distance Δ is given by (30) as $\Delta > 0.15$ m. During the simulation, we chose the look-ahead distance as $\Delta = 1.4$ m, which equals the length of the snake robot, and which is well above the estimated lower limit.

The derivatives $\dot{\phi}_o$, $\ddot{\phi}_o$, $\dot{\theta}_{\text{ref}}$, and $\ddot{\theta}_{\text{ref}}$, which are needed for the calculation of the control input in (22) and (27), were obtained by passing ϕ_o and θ_{ref} through a 3rd order low-pass filtering reference model (see e.g. Chapter 5 in [38]).

The initial state of the snake robot was chosen as $\boldsymbol{\phi} = \mathbf{0}°$, $\theta = 90°$, $p_x = 0$ m, $p_y = 1$ m, $\boldsymbol{v}_\phi = \mathbf{0}°$/s, $v_\theta = 0°$/s, $v_t = 0.1$ m/s, and $v_n = 0$ m/s, i.e. the snake robot was initially oriented along the global y axis and located 1 m away from the x axis with an initial forward velocity of 0.1 m/s, i.e. moving away from the desired path.

B. Simulation Results

The simulation results are shown in Fig. 6. From Figures 6(a)-(b), we see that the position of the snake robot converges nicely to the desired path (i.e. the x axis). Fig. 6(a) shows the configuration of the snake robot at $t = 1$ s, $t = 30$ s, and $t = 70$ s. Note that Fig. 6(b) shows the cross-track error in terms of the y axis coordinate of the CM of the robot, not the transformed y-axis coordinate given by (15b). The heading of the snake robot, shown in Fig. 6(c), also converges nicely to zero, i.e. to the direction of the desired path. As seen in Fig. 6(e), the forward velocity is always nonzero and positive, as required by Assumption 9, and converges to the velocity $v_t^* = \frac{c_2}{2Nc_1}\alpha^2\omega k_\delta = 0.1$ m/s, which was estimated above. Fig. 6(f) shows the joint coordinate of an arbitrarily chosen joint (joint 5) during the path following. The plot shows a very good tracking of the corresponding joint reference coordinates. In summary, the simulation results illustrate that the proposed path following controller successfully steers the snake robot towards and along the desired straight path.

VI. Experimental study

In this section, we present results from an experimental investigation of the performance of the proposed path following controller.

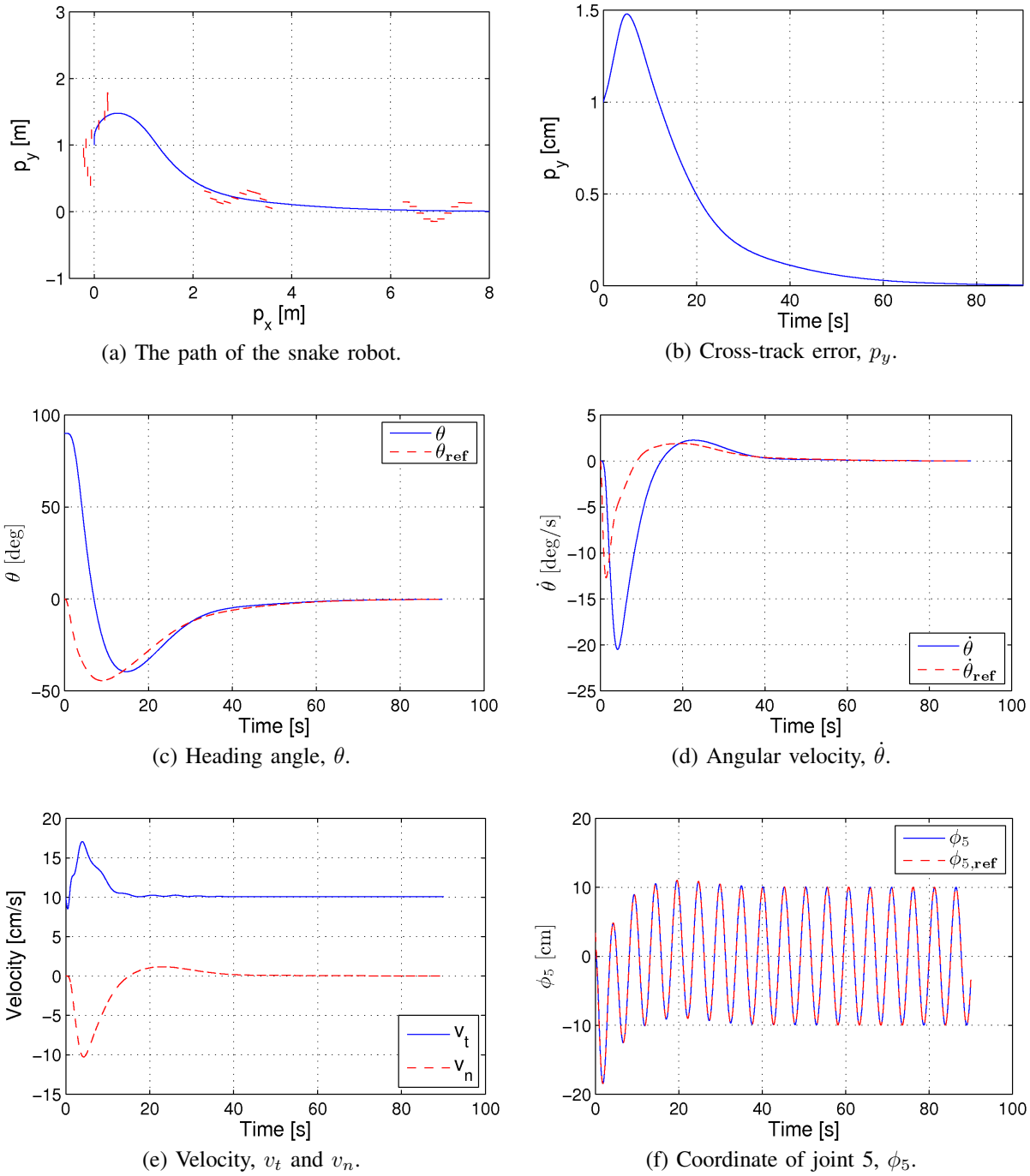

(a) The path of the snake robot.

(b) Cross-track error, p_y.

(c) Heading angle, θ.

(d) Angular velocity, $\dot{\theta}$.

(e) Velocity, v_t and v_n.

(f) Coordinate of joint 5, ϕ_5.

Fig. 6. Simulation of straight line path following with the snake robot initially headed away from the desired path.

A. The snake robot

The snake robot used in the experiments is shown in Fig. 7. A detailed description of the internal components of the robot is given in [42]. The snake robot consists of 10 identical joint modules characterized by the parameters listed in Table II. Each joint module has 2 degrees of freedom (pitch and yaw motion) driven by two Hitec servo motors (HS-5955TG). The pitch and yaw angle of the joint modules are measured with magnetic rotary encoders (AS5043 from austriamicrosystems).

As shown to the left in Fig. 9, each joint module is covered by 12 small wheels. These wheels ensure that the ground friction forces acting on the snake robot are *anisotropic*, i.e. that the friction coefficient characterizing the ground friction forces in the normal (sideways) direction of each joint is larger than the tangential (forward) direction friction coefficient. This property is essential for efficient snake locomotion on a planar surface and is also present in the model of the snake robot (11). Note that the wheels are able to slip sideways, so they do not introduce nonholonomic constraints in the system.

Each joint module is battery-powered and contains a custom-designed microcontroller card used to control the joint angles. A microcontroller card (the brain card) located in the

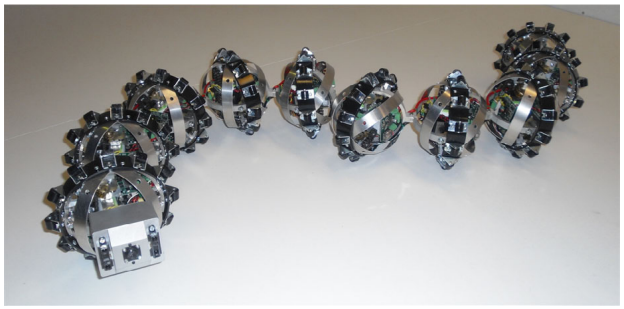

Fig. 7. The snake robot used in the experiment.

TABLE II
PARAMETERS OF A JOINT MODULE.

Parameter	Value
Total weight of a joint module	960 g
Outer diameter	130 mm
Degrees of freedom	2
Max joint travel	$\pm 45^\circ$
Max continuous joint torque	4.5 Nm
Max joint speed (no load)	$70^\circ/_{\text{sec}}$

head of the snake robot transmits joint reference angles to all joint modules over a CAN bus running through the robot. The joint reference angles are calculated on an external computer and sent to the brain card via a wireless connection based on Bluetooth. The refresh rate for the two reference angles of each joint module is about 20 Hz.

B. The camera-based position measurement system

During the experiments, the snake robot moved on a white horizontal surface measuring about 240 cm in width and 600 cm in length. This is shown in Fig. 8. The 2D position of the robot was measured by use of the open source camera tracking software *SwisTrack* [43]. SwisTrack was configured to read camera data at 15 frames per second from three firewire cameras (Unibrain Fire-i 520c) mounted in the ceiling above the snake robot as shown in Fig. 8. The use of multiple cameras allowed for position measurements over a greater distance than the area covered by a single camera. The cameras were mounted facing downwards approximately 218 cm above the floor and 132 cm apart.

SwisTrack was configured to track black circular markers (40 mm in diameter) mounted on the snake robot as shown to the right in Fig. 9. The conversion from the pixel position of a marker to the real-world position (in cm) was conducted by SwisTrack based on a specific calibration method available in this software. SwisTrack estimated the maximum position error to be about 1.9 cm and the average position error to be about 0.6 cm. The global frame position, x_{head} and y_{head}, and the angle, θ_{head}, of the head of the snake robot were calculated from the individual marker positions. Knowing the position and orientation of the head, and also the individual joint angles, we employed simple kinematic relationships presented in [18] in order to calculate the position of the center of mass, p_x and p_y, of the snake robot. The orientation, which for the physical robot is denoted by $\overline{\theta}$, was estimated as the average of the individual absolute link angles. Furthermore, the forward velocity, which for the physical robot is denoted by $\overline{v}_t$, was

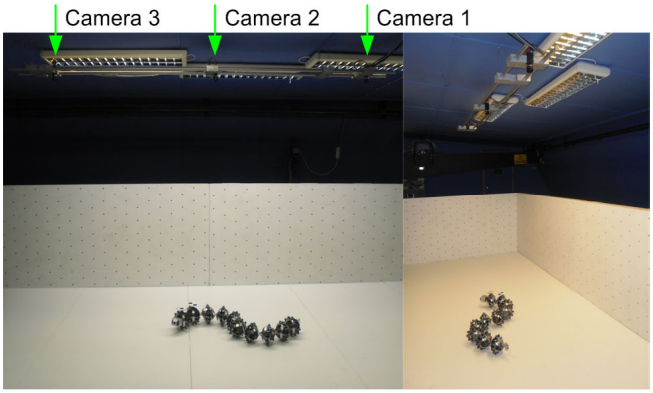

Fig. 8. The experimental setup. Three cameras mounted in the ceiling measured the position of the snake robot on a horizontal surface measuring about 240 cm in width and 600 cm in length.

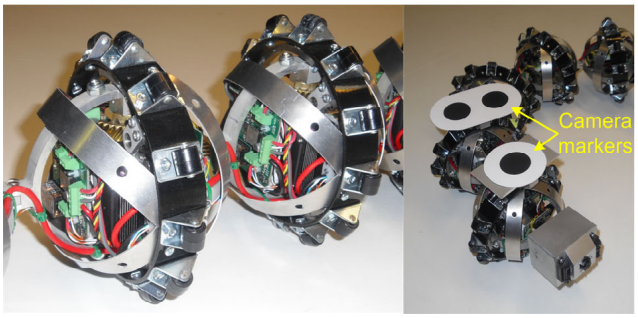

Fig. 9. Left: The wheels installed around each joint module in order to give the robot anisotropic ground friction properties. Right: The black markers mounted on the snake robot to allow the position to be tracked by SwisTrack.

estimated at 0.5 Hz as the displacement of the CM of the robot divided by the sampling interval (i.e. 2 s). The sampling interval was chosen to be large to obtain a reasonably accurate velocity estimate, but was sufficiently short for the experiment since the robot was moved at a slow pace.

C. Implementation of the path following controller

The controller of the physical snake robot was implemented on an external computer according to (19), (25), and (27). We did not implement the joint torque controller given by (21) and (22) since accurate torque control is not supported by the servo motors installed in the snake robot. The joint angles were instead controlled according to a proportional controller implemented in the microcontroller of each joint module. Note that we can experimentally validate Theorem 13 without implementing the joint controller (21) and (22) since, as stated in Remark 19, the global $\mathcal{K}$-exponential stability of the complete system only requires that the error dynamics of the joints is exponentially stabilized.

The simplified model describes the *qualitative* behaviour of a snake robot with revolute joints, and also approximates the *quantitative* behaviour of the robot for some choice of the ground friction coefficients c_1, c_2, c_3, and c_4. However, no definite mapping exists between the ground friction coefficients of a snake robot with revolute joints and the friction coefficients c_1 - c_4. In other words, the values of c_1 - c_4 that reflected the specific ground friction conditions of the experiments were not know. Since c_3 and c_4 appear in the equations of the path

following controller, we chose to treat these coefficients as controller gains.

The unspecified values of c_1 - c_4 prevented us from determining the coordinate transformation distance ϵ in (16), which depends on c_2 and c_4. During the experiments, we therefore set this coordinate transformation distance to $\epsilon = 0$, i.e. we measured the cross-track error as $\overline{p}_y = p_y$. Note that since the ϵ transformation is tangential to the robot, the value of ϵ has only a limited effect on the cross-track error when the heading of the snake robot with respect to the path is close to zero.

The LOS angle $\theta_{\rm ref}$ given by (25) was calculated with a look-ahead distance Δ equal to half the length of the snake robot, i.e. $\Delta = 0.7$ m. We conjecture that this value is well above the lower limit of Δ given by (30). The actual values of $V_{\min}$ and $V_{\max}$ are not known a priori, and as noted in Remark 14, specifying the bounds on Δ as a function of the gait pattern parameters α, ω, δ, and ϕ_o remains a topic of future work. Note that $\Delta = 0.7$ m is well above the lower value of Δ estimated for the simulated snake robot in Section V (i.e. $\Delta > 0.15$ m), although this lower bound estimate was not based on friction coefficients corresponding to the ground friction conditions of the experiment, which are unknown, as described above.

To ensure a smooth control input, the LOS angle $\theta_{\rm ref}$ was passed through a 3rd order low-pass filtering reference model (see e.g. Chapter 5 in [38]). The output from this filter also provided the derivatives $\dot{\theta}_{\rm ref}$ and $\ddot{\theta}_{\rm ref}$, which are required in the calculation of ϕ_o in (27). The evolution of the reference values from the filter were calculated with a first-order numerical integration scheme.

The joint angle offset ϕ_o given by (27) was calculated with the controller gains set to $k_\theta = 1$, $c_3 = 0.5$ and $c_4 = 20$. The joint angle offset was saturated according to $\phi_o \in [-25^\circ, 25^\circ]$ in order to keep the joint reference angles within reasonable bounds with respect to the maximum allowable joint angles of the physical snake robot. This saturation also avoided the singularity in (27) at $\overline{v}_t = 0$ (see Remark 11). Furthermore, to ensure that the joint angle offset was smooth despite of any steps in the estimate of the forward velocity $\overline{v}_t$, we filtered ϕ_o with a 1st order low-pass filter with cutoff frequency set to 1.25 Hz.

The reference angles corresponding to the horizontal joint motion of the robot were calculated according to (19) with $N = 10$ links and with gait parameters set to $\alpha = 30^\circ$, $\omega = 50^\circ$/s, and $\delta = 36^\circ$. The reference angles corresponding to the vertical joint motion were set to zero to achieve a purely planar locomotion.

D. Experimental results

The straight line path following controller was experimentally investigated from two different sets of initial conditions. In the first trial, the initial state of the snake robot was approximately $\boldsymbol{\phi} = \mathbf{0}^\circ$, $\theta = 0^\circ$, $p_x = 0$ m, $p_y = 1.3$ m, $\boldsymbol{v}_\phi = \mathbf{0}^\circ$/s, $v_\theta = 0^\circ$/s, $v_t = 0$ m/s, and $v_n = 0$ m/s, i.e. the snake robot was initially headed *along* the desired path (the x axis) and the initial distance from the CM to the desired path was 1.3 m. In the second trial, the initial state of the robot was approximately $\boldsymbol{\phi} = \mathbf{0}^\circ$, $\theta = 90^\circ$, $p_x = 0$ m, $p_y = 0.5$ m, $\boldsymbol{v}_\phi = \mathbf{0}^\circ$/s, $v_\theta = 0^\circ$/s, $v_t = 0$ m/s, and $v_n = 0$ m/s, i.e. the snake robot was initially headed *away* from the desired path (the x axis) and the initial distance from the CM to the desired path was 0.5 m.

The experimentally measured motion of the snake robot from the first trial is presented in Figures 10(a) and 11, and from the second trial in Figures 10(b) and 12. The desired path, i.e. the global x axis, is indicated with a black line on the floor in the pictures of the snake robot during the two trials.

The visualizations in Fig. 10 indicate that the snake robot converged nicely towards and along the desired path during both trials. This claim is supported by the plots of the cross-track error in Figures 11(b) and 12(b), which show that the cross-track error converges to and oscillates about zero. For a snake robot with revolute joints, it is difficult to achieve a purely non-oscillating motion of the CM, which was achieved in the simulation results based on the simplified model in Section V. We therefore expected the cross-track error to oscillate about zero, as seen in the plots, rather than converge to zero.

Similar to the oscillatory behaviour of the CM, the heading $\overline{\theta}$ of the snake robot was also expected to oscillate. In particular, while θ provides an explicit representation of the heading in the simplified model, such a representation is not available for a snake robot with revolute joints, which forced us to estimate the heading according to $\overline{\theta}$, i.e. as the average of the link angles. The oscillatory behaviour of $\overline{\theta}$ was thereby expected since the average of the link angles will not always be identically zero during forward locomotion. The heading during the trials is shown in Figures 11(c) and 12(c), respectively, which clearly show that $\overline{\theta}$ oscillates nicely about the reference heading $\overline{\theta}_{\rm ref}$. In both trials, the heading converges to and oscillates about zero, i.e. the direction of the desired path.

The forward velocity of the robot during the trials is shown in Figures 11(d) and 12(d), respectively. The variations in the velocity were primarily caused by the joint angle offset ϕ_o during turning motion, which sometimes interfered with the oscillatory body wave motion and caused the robot to lose momentum.

The joint angle of an arbitrarily chosen joint (joint 5) during each trial is shown in Figures 11(f) and 12(f), respectively, which indicate that the snake robot tracked its joint reference coordinates very well.

In summary, the proposed path following controller successfully steered the snake robot towards and along the desired straight path during both trials of the experiment.

VII. Conclusions

This paper has proposed a path following controller that enables snake robots to track straight paths. Using cascaded systems theory, we have proven that the proposed path following controller $\mathcal{K}$-exponentially stabilizes the snake robot to any desired straight path under the assumption that the forward velocity of the robot is nonzero and positive. The performance of the path following controller was investigated through simulations and through experiments with a physical snake robot where the proposed controller was shown to successfully steer the snake robot towards and along the desired straight path.

In future work, the authors will seek to specify the bounds on the forward velocity of the snake robot in terms of the gait pattern parameters.

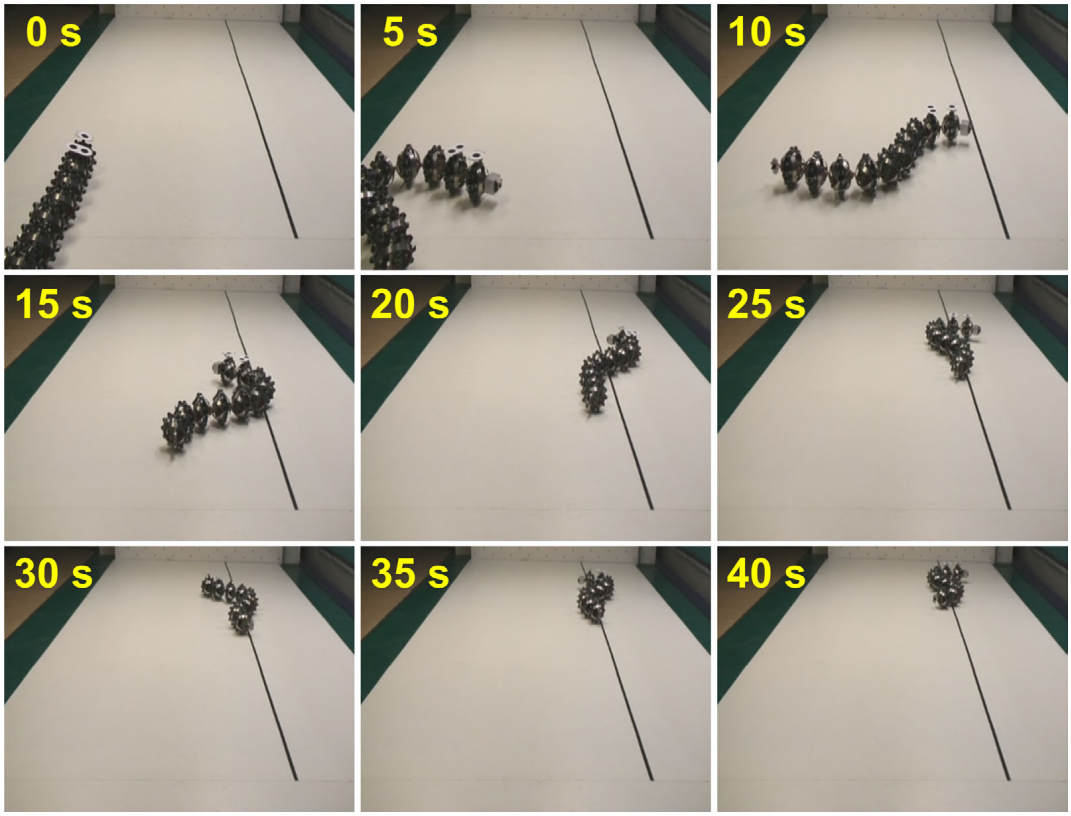

(a) Path following with an initial heading along the desired path.

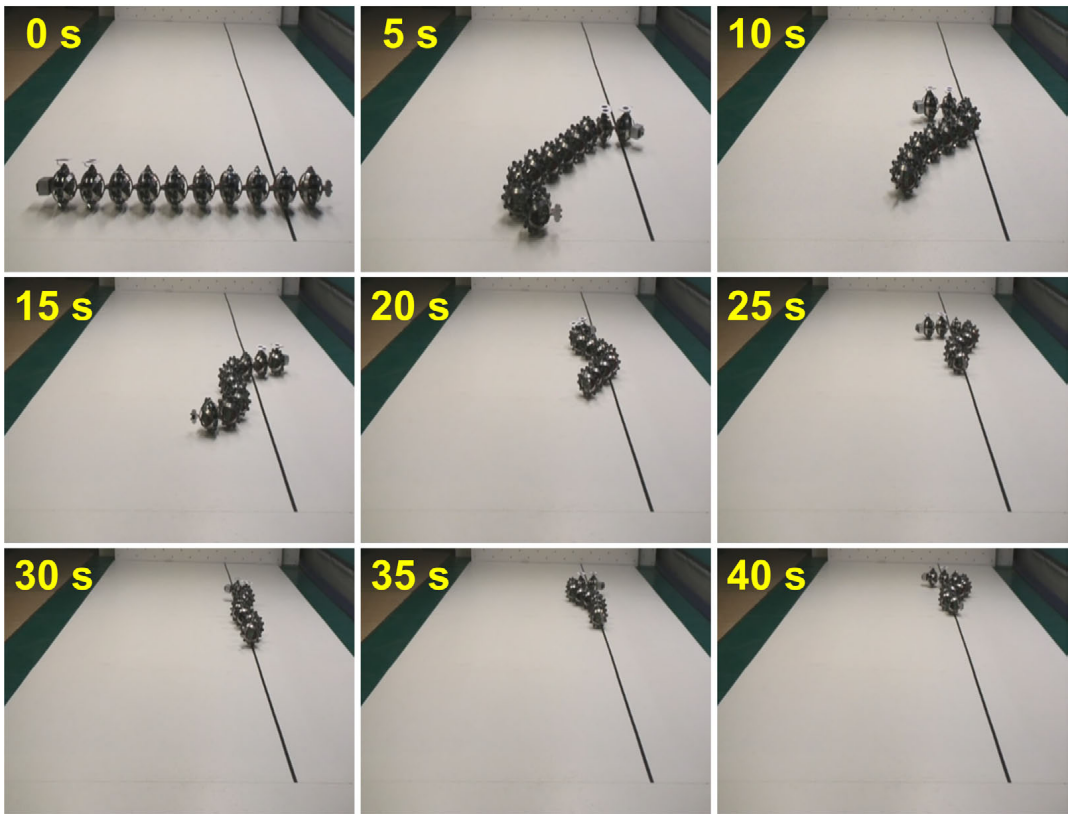

(b) Path following with an initial heading away from the desired path.

Fig. 10. The motion of the physical snake robot during path following from two different sets of initial conditions. The black line on the floor indicates the desired path, i.e. the global x axis.

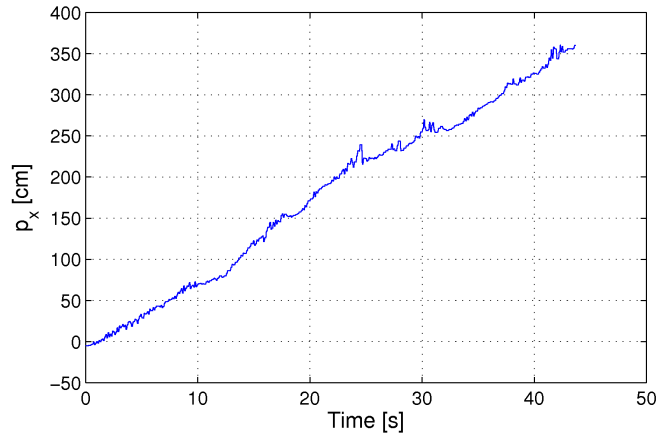

(a) Position along the path, p_x.

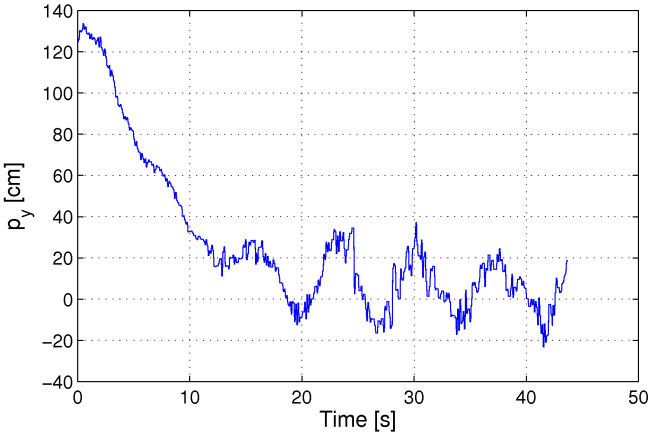

(b) Cross-track error, p_y.

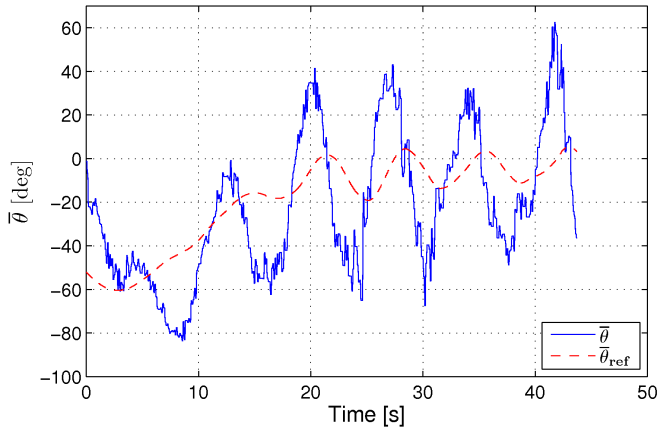

(c) Heading angle, $\overline{\theta}$.

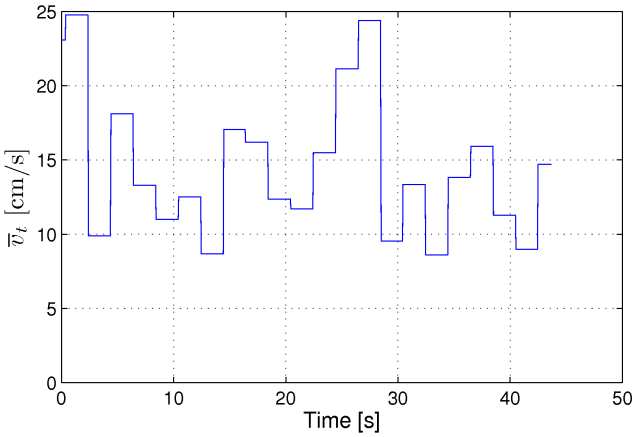

(d) Forward velocity, $\overline{v}_t$.

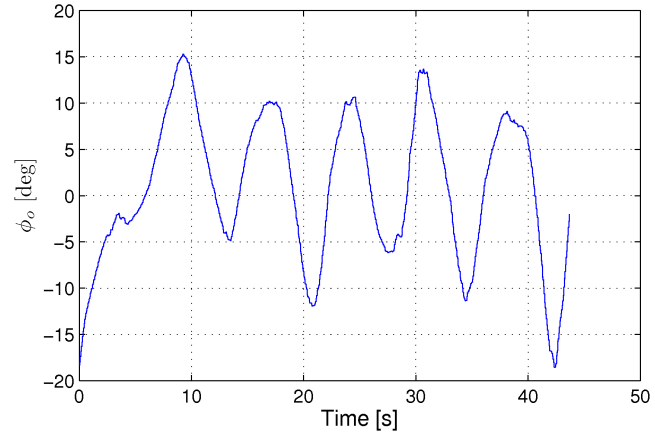

(e) Joint angle offset, ϕ_o.

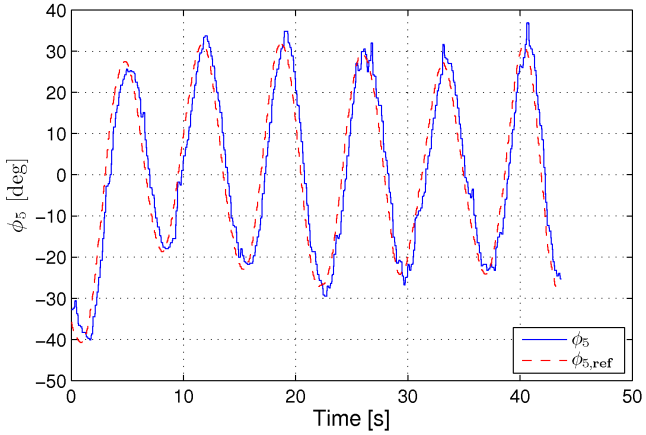

(f) Angle of joint 5, ϕ_5.

Fig. 11. Straight line path following with the physical snake robot initially headed along the desired path.

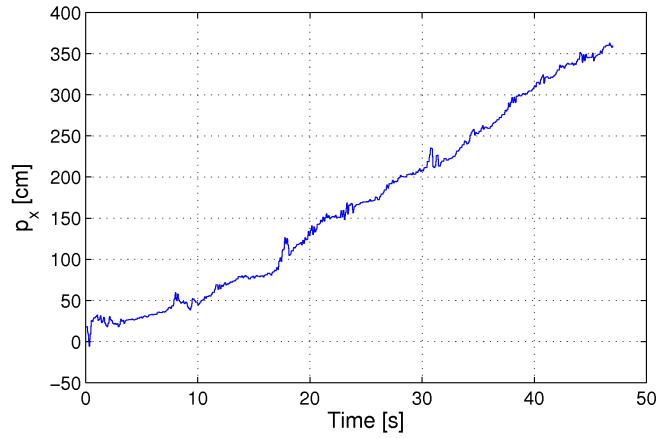

(a) Position along the path, p_x.

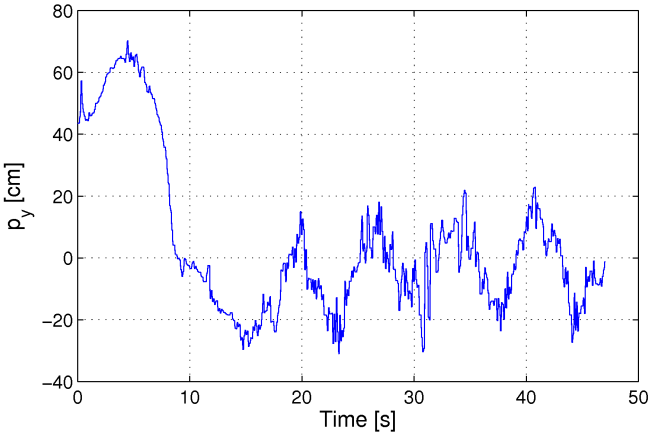

(b) Cross-track error, p_y.

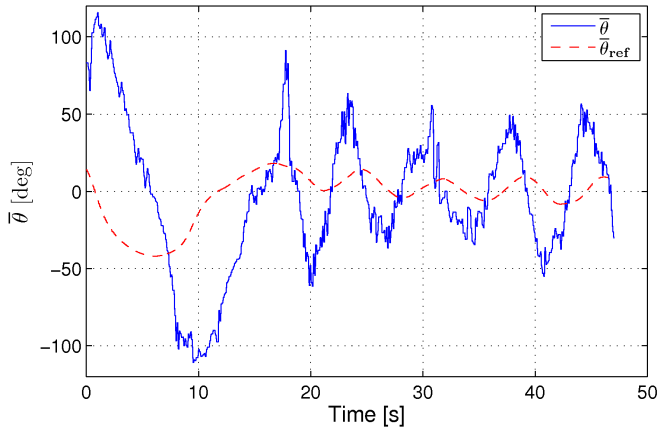

(c) Heading angle, $\overline{\theta}$.

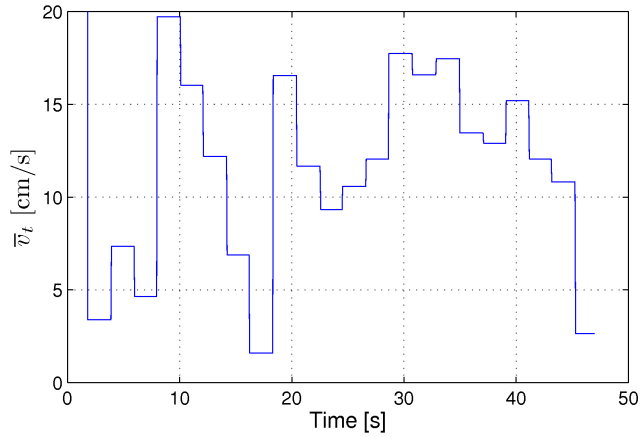

(d) Forward velocity, $\overline{v}_t$.

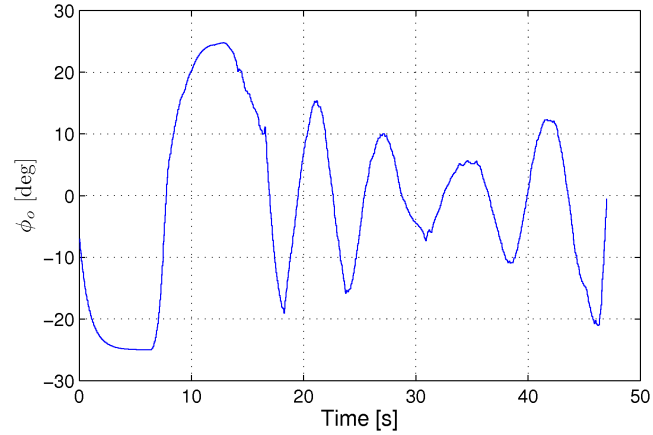

(e) Joint angle offset, ϕ_o.

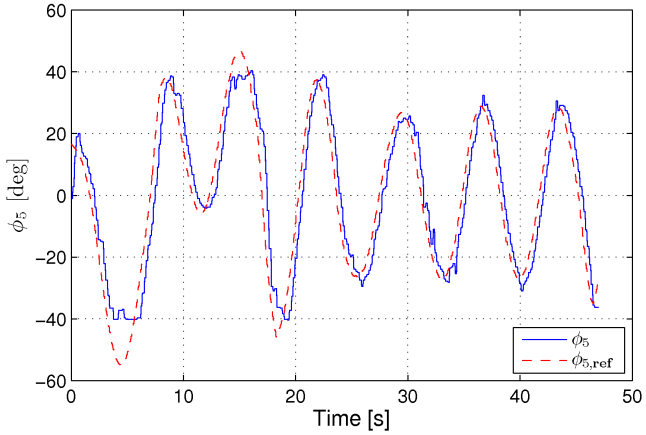

(f) Angle of joint 5, ϕ_5.

Fig. 12. Straight line path following with the physical snake robot initially headed away from the desired path.

APPENDIX A
PROOF OF LEMMA 17

The proof of Lemma 17 has previously been presented in [41] and is included here for completeness. The Lemma is proved by showing that a quadratic Lyapunov function candidate of the system (41) is negative definite, thereby implying that (41) is UGAS.

The system (41) can be written as

$$\begin{bmatrix}\dot{\overline{p}}_y\\ \dot{\overline{v}}_n\end{bmatrix} = \begin{bmatrix} -\frac{v_t}{\sqrt{\overline{p}_y^2+\Delta^2}} & \frac{\Delta}{\sqrt{\overline{p}_y^2+\Delta^2}} \\ \frac{X\Delta v_t}{\left(\sqrt{\overline{p}_y^2+\Delta^2}\right)^3} & \left(Y-\frac{X\Delta^2}{\left(\sqrt{\overline{p}_y^2+\Delta^2}\right)^3}\right)\end{bmatrix}\begin{bmatrix}\overline{p}_y\\ \overline{v}_n\end{bmatrix}. \quad (48)$$

Consider the quadratic Lyapunov function candidate $V = 1/2\overline{p}_y^2 + \kappa/2\overline{v}_n^2$ with $\kappa > 0$. The derivative of V along the solutions of (48) is given by

$$\begin{aligned}\dot{V} = \overline{p}_y\dot{\overline{p}}_y + \kappa\overline{v}_n\dot{\overline{v}}_n = -\frac{v_t\overline{p}_y^2}{\sqrt{\overline{p}_y^2+\Delta^2}} + \frac{\Delta\overline{p}_y\overline{v}_n}{\sqrt{\overline{p}_y^2+\Delta^2}} \\ +\kappa\frac{X\Delta v_t\overline{p}_y\overline{v}_n}{\left(\sqrt{\overline{p}_y^2+\Delta^2}\right)^3} + \kappa\left(Y-\frac{X\Delta^2}{\left(\sqrt{\overline{p}_y^2+\Delta^2}\right)^3}\right)\overline{v}_n^2.\end{aligned} \quad (49)$$

Since $v_t \in [V_{\min}, V_{\max}]$ by Assumption 9, and since $X \le |X|$, we can estimate $\dot{V}$ as

$$\begin{aligned}\dot{V} \le -\frac{V_{\min}\overline{p}_y^2}{\sqrt{\overline{p}_y^2+\Delta^2}} + \frac{\Delta\overline{p}_y\overline{v}_n}{\sqrt{\overline{p}_y^2+\Delta^2}} \\ +\kappa\frac{|X|\Delta V_{\max}\overline{p}_y\overline{v}_n}{\left(\sqrt{\overline{p}_y^2+\Delta^2}\right)^3} + \kappa\left(Y+\frac{|X|\Delta^2}{\left(\sqrt{\overline{p}_y^2+\Delta^2}\right)^3}\right)\overline{v}_n^2.\end{aligned} \quad (50)$$

By introducing the variable $z = \left|\overline{p}_y\right| / \sqrt{\overline{p}_y^2+\Delta^2}$, this estimate can be written as

$$\begin{aligned}\dot{V} \le -V_{\min}z^2\sqrt{\overline{p}_y^2+\Delta^2} \\ +\left(\Delta+\kappa\frac{|X|\Delta V_{\max}}{\overline{p}_y^2+\Delta^2}\right)z\left|\overline{v}_n\right| + \kappa\left(Y+\frac{|X|\Delta^2}{\left(\sqrt{\overline{p}_y^2+\Delta^2}\right)^3}\right)\overline{v}_n^2.\end{aligned} \quad (51)$$

Finally, using the inequalities $-\sqrt{\overline{p}_y^2+\Delta^2} \le -\Delta$ and $1/\left(\overline{p}_y^2+\Delta^2\right) \le 1/\Delta^2$, we obtain

$$\begin{aligned}\dot{V} \le -V_{\min}\Delta z^2 \\ +\left(\Delta+\kappa\frac{|X|V_{\max}}{\Delta}\right)z\left|\overline{v}_n\right| + \kappa\left(Y+\frac{|X|}{\Delta}\right)\overline{v}_n^2.\end{aligned} \quad (52)$$

We now choose $\kappa = \Delta^2(2\beta-1)/(|X|V_{\max})$, where

$$\beta = \frac{V_{\min}(-\Delta Y - |X|)}{V_{\max}|X|}. \quad (53)$$

It is straightforward to show that condition (30) of Theorem 13 is equivalent to $\beta > 1$. The chosen value of κ is therefore strictly positive. Substituting this κ into (52) gives

$$\begin{aligned}\dot{V} &\le -V_{\min}\Delta z^2 + 2\beta\Delta z\left|\overline{v}_n\right| - \frac{\Delta(2\beta-1)\beta}{V_{\min}}\overline{v}_n^2 \\ &= -\Delta\left(\sqrt{V_{\min}}z - \frac{\beta|\overline{v}_n|}{\sqrt{V_{\min}}}\right)^2 - \frac{\Delta(\beta-1)\beta}{V_{\min}}\overline{v}_n^2.\end{aligned} \quad (54)$$

Finally, substituting the expression for z into this estimate gives

$$\dot{V} \le -\Delta\left(\frac{\sqrt{V_{\min}}\left|\overline{p}_y\right|}{\sqrt{\overline{p}_y^2+\Delta^2}} - \frac{\beta\left|\overline{v}_n\right|}{\sqrt{V_{\min}}}\right)^2 - \frac{\Delta(\beta-1)\beta}{V_{\min}}\overline{v}_n^2. \quad (55)$$

Since condition (30) guarantees that $\beta > 1$, we can conclude that $\dot{V} < 0$, which implies that the origin of the system (41) is UGAS (see [24]). This completes the proof of Lemma 17.

APPENDIX B
PROOF OF LEMMA 18

The lemma is proved by showing that the system (41) is ULES (uniformly locally exponentially stable), which, together with the UGAS property established by Lemma 17, implies that (41) is globally $\mathcal{K}$-exponentially stable according to Corollary 4.

The linearization of the system (41) about the origin is easily calculated as

$$\begin{bmatrix}\dot{\overline{p}}_y\\ \dot{\overline{v}}_n\end{bmatrix} = \begin{bmatrix} -\frac{v_t}{\Delta} & 1 \\ \frac{Xv_t}{\Delta^2} & Y-\frac{X}{\Delta}\end{bmatrix}\begin{bmatrix}\overline{p}_y\\ \overline{v}_n\end{bmatrix}. \quad (56)$$

Denoting the system matrix of (56) by $\boldsymbol{W}$, we can calculate the eigenvalues of $\boldsymbol{W}$ from its characteristic equation

$$\lambda^2 - \mathrm{tr}(\boldsymbol{W})\lambda + \det(\boldsymbol{W}) = 0, \quad (57)$$

where $\mathrm{tr}(\boldsymbol{W})$ and $\det(\boldsymbol{W})$ are the trace and the determinant of $\boldsymbol{W}$, respectively. $\boldsymbol{W}$ is Hurwitz (see e.g. [24]) if the coefficients of this characteristic equation are strictly positive, i.e. if $\mathrm{tr}(\boldsymbol{W}) < 0$ and $\det(\boldsymbol{W}) > 0$. Since $v_t > 0$, $Y < 0$, and $\Delta > 2|X|/|Y|$ (this follows from (30)), the trace of $\boldsymbol{W}$ satisfies

$$\begin{aligned}\mathrm{tr}(\boldsymbol{W}) = -\frac{v_t}{\Delta} + Y - \frac{X}{\Delta} \le -\frac{v_t}{\Delta} - |Y| + \frac{|X|}{\Delta} \\ \le -\frac{v_t}{\Delta} - |Y| + \frac{1}{2}|Y| = -\frac{v_t}{\Delta} - \frac{1}{2}|Y| < 0,\end{aligned} \quad (58)$$

and the determinant of $\boldsymbol{W}$ satisfies

$$\det(\boldsymbol{W}) = -\frac{v_t}{\Delta}\left(Y-\frac{X}{\Delta}\right) - \frac{Xv_t}{\Delta^2} = -\frac{v_t}{\Delta}Y > 0. \quad (59)$$

The system matrix $\boldsymbol{W}$ of the linearized system (56) is therefore Hurwitz, which implies that the origin of the system (41) is ULES (see [24], Corollary 4.3). Since, by Lemma 17, the origin of (41) is also UGAS, Corollary 4 implies that the origin of (41) is globally $\mathcal{K}$-exponentially stable. This completes the proof of Lemma 18.

REFERENCES

[1] J. Gray, "The mechanism of locomotion in snakes," *J. Exp. Biol.*, vol. 23, no. 2, pp. 101–120, 1946.

[2] S. Hirose, *Biologically Inspired Robots: Snake-Like Locomotors and Manipulators*. Oxford: Oxford University Press, 1993.

[3] J. W. Burdick, J. Radford, and G. Chirikjian, "A sidewinding locomotion gait for hyper-redundant robots," *Advanced Robotics*, vol. 9, no. 3, pp. 195–216, 1995.

[4] G. Chirikjian and J. Burdick, "The kinematics of hyper-redundant robot locomotion," *IEEE Trans. Robot. Autom.*, vol. 11, no. 6, pp. 781–793, December 1995.

[5] R. L. Hatton and H. Choset, "Sidewinding on slopes," in *IEEE Int. Conf. Robotics and Automation*, 2010, pp. 691–696.

[6] G. S. P. Miller, "The motion dynamics of snakes and worms," *Computer Graphics*, vol. 22, no. 4, pp. 163–173, Aug 1988.

[7] M. Yim, "New locomotion gaits," in *Proc. IEEE Int. Conf. on Robotics and Automation*, vol. 3, May 1994, pp. 2508–2514.

[8] M. Tesch, K. Lipkin, I. Brown, R. Hatton, A. Peck, J. Rembisz, and H. Choset, "Parameterized and scripted gaits for modular snake robots," *Advanced Robotics*, vol. 23, no. 9, pp. 1131–1158, 2009.

[9] S. Ma, "Analysis of creeping locomotion of a snake-like robot," *Adv. Robotics*, vol. 15, no. 2, pp. 205–224, 2001.

[10] M. Saito, M. Fukaya, and T. Iwasaki, "Serpentine locomotion with robotic snakes," *IEEE Contr. Syst. Mag.*, vol. 22, no. 1, pp. 64–81, February 2002.

[11] Z. Y. Bayraktaroglu, "Snake-like locomotion: Experimentations with a biologically inspired wheel-less snake robot," *Mechanism and Machine Theory*, vol. 44, no. 3, pp. 591–602, 2008.

[12] P. Liljebäck, K. Y. Pettersen, Ø. Stavdahl, and J. T. Gravdahl, "Hybrid modelling and control of obstacle-aided snake robot locomotion," *IEEE Trans. Robotics*, vol. 26, no. 5, pp. 781–799, Oct 2010.

[13] P. Prautsch, T. Mita, and T. Iwasaki, "Analysis and control of a gait of snake robot," *Trans. IEE J. Ind. Appl. Soc.*, vol. 120-D, pp. 372–381, 2000, mer utfyllende versjon av "Control and Analysis of the Gait of Snake Robots" (Prautsch1999).
[14] H. Date, Y. Hoshi, and M. Sampei, "Locomotion control of a snake-like robot based on dynamic manipulability," in *Proc. IEEE/RSJ Int. Conf. Intelligent Robots and Systems*, 2000.
[15] M. Yamakita, M. Hashimoto, and T. Yamada, "Control of locomotion and head configuration of 3d snake robot (sma)," in *Proc. IEEE Int. Conf. Robotics and Automation*, vol. 2, Taipei, Taiwan, 2003, pp. 2055 – 2060. [Online]. Available: http://dx.doi.org/10.1109/ROBOT.2003.1241896
[16] F. Matsuno and H. Sato, "Trajectory tracking control of snake robots based on dynamic model," in *Proc. IEEE Int. Conf. on Robotics and Automation*, 2005, pp. 3029–3034.
[17] B. Murugendran, A. A. Transeth, and S. A. Fjerdingen, "Modeling and path-following for a snake robot with active wheels," in *Proc. IEEE/RSJ Int. Conf. Intelligent Robots and Systems*, 2009, pp. 3643 – 3650.
[18] P. Liljebäck, K. Y. Pettersen, Ø. Stavdahl, and J. T. Gravdahl, "Controllability and stability analysis of planar snake robot locomotion," *IEEE Trans. Automatic Control*, 2011, to appear.
[19] P. A. Vela, K. A. Morgansen, and J. W. Burdick, "Underwater locomotion from oscillatory shape deformations," in *Proc. IEEE Conf. Decision and Control*, vol. 2, Dec. 2002, pp. 2074–2080 vol.2.
[20] K. McIsaac and J. Ostrowski, "Motion planning for anguilliform locomotion," *IEEE Trans. Rob. Aut.*, vol. 19, no. 4, pp. 637–625, 2003.
[21] K. Morgansen, B. Triplett, and D. Klein, "Geometric methods for modeling and control of free-swimming fin-actuated underwater vehicles," *IEEE Trans. Robotics*, vol. 23, no. 6, pp. 1184–1199, Dec 2007.
[22] P. Liljebäck, I. U. Haugstuen, and K. Y. Pettersen, "Path following control of planar snake robots using a cascaded approach," in *Proc. IEEE Conf. Decision and Control*, Atlanta, GA, USA, 2010, pp. 1969–1976.
[23] ——, "Experimental investigation of a path following controller for planar snake robots," in *Proc. IEEE Int. Conf. Control, Automation, Robotics, and Vision (ICARCV)*, Singapore, 2010, pp. 2325–2332.
[24] H. K. Khalil, *Nonlinear Systems*, 3rd ed. Prentice Hall, 2002.
[25] O. J. Sørdalen and O. Egeland, "Exponential stabilization of nonholonomic chained systems," *IEEE Trans. Automatic Control*, vol. 40, no. 1, pp. 35 – 49, 1995.
[26] E. Lefeber, "Tracking control of nonlinear mechanical systems," Ph.D. dissertation, University of Twente. The Netherlands., 2000.
[27] E. Panteley and A. Loria, "On global uniform asymptotic stability of nonlinear time-varying systems in cascade," *Systems & Control Letters*, vol. 33, no. 2, pp. 131 – 138, 1998.
[28] E. Panteley, E. Lefeber, A. Loria, and H. Nijmeijer, "Exponential tracking control of a mobile car using a cascaded approach," in *Proc. IFAC Workshop on Motion Control*, 1998, pp. 221 – 226.
[29] P. Liljebäck, K. Y. Pettersen, Ø. Stavdahl, and J. T. Gravdahl, "A simplified model of planar snake robot locomotion," in *Proc. IEEE/RSJ Int. Conf. Intelligent Robots and Systems*, Taipei, Taiwan, 2010, pp. 2868–2875.
[30] G. Chirikjian, "Hyper-redundant manipulator dynamics: a continuum approximation," *Advanced robotics*, vol. 9, no. 3, pp. 217–243, 1995.
[31] H. Date and Y. Takita, "Control of 3d snake-like locomotive mechanism based on continuum modeling," in *Proc. ASME 2005 International Design Engineering Technical Conferences*, 2005, no. DETC2005-85130.
[32] H. Yamada and S. Hirose, "Study on the 3d shape of active cord mechanism," in *Proc. IEEE Int. Conf. Robotics and Automation*, 2006, pp. 2890–2895.
[33] R. Hatton and H. Choset, "Approximating displacement with the body velocity integral," in *Proc. Robotics: Science and Systems*, 2009.
[34] D. Hu, J. Nirody, T. Scott, and M. Shelley, "The mechanics of slithering locomotion," in *Proc. National Academy of Sciences, USA*, vol. 106, 2009, p. 10081 10085.
[35] P. Liljebäck, K. Y. Pettersen, Ø. Stavdahl, and J. T. Gravdahl, "Stability analysis of snake robot locomotion based on averaging theory," in *Proc. IEEE Conf. Decision and Control*, Atlanta, GA, USA, 2010, pp. 1977–1984.
[36] K. Do and J. Pan, "Global tracking control of underactuated ships with off-diagonal terms," in *IEEE Conf. Decision and Control*, vol. 2, 2003, pp. 1250–1255.
[37] P. Liljebäck, K. Y. Pettersen, Ø. Stavdahl, and J. T. Gravdahl, "Fundamental properties of snake robot locomotion," in *Proc. IEEE/RSJ Int. Conf. Intelligent Robots and Systems*, Taipei, Taiwan, 2010, pp. 2876–2883.
[38] T. I. Fossen, *Marine Control Systems: Guidance, Navigation and Control of Ships, Rigs and Underwater Vehicles*. Trondheim, Norway: Marine Cybernetics, 2002.
[39] E. Fredriksen and K. Y. Pettersen, "Global κ-exponential way-point maneuvering of ships: Theory and experiments," *Automatica*, vol. 42, pp. 677 – 687, 2006.
[40] K. Y. Pettersen and E. Lefeber, "Way-point tracking control of ships," in *Proc. IEEE Conf. Decision and Control*, 2001, pp. 940–945.
[41] A. Pavlov, E. Børhaug, E. Panteley, and K. Y. Pettersen, "Straight line path following for formations of underactuated surface vessels," in *Proc. IFAC NOLCOS*, 2007.
[42] P. Liljebäck, K. Y. Pettersen, and Ø. Stavdahl, "A snake robot with a contact force measurement system for obstacle-aided locomotion," in *Proc. IEEE Int. Conf. Robotics and Automation*, Anchorage, AK, USA, 2010, pp. 683–690.
[43] T. Lochmatter, P. Roduit, C. Cianci, N. Correll, J. Jacot, and A. Martinoli, "Swistrack - a flexible open source tracking software for multi-agent systems," in *IEEE/RSJ Int. Conf. Intelligent Robots and Systems*, 2008, pp. 4004–4010.

Pål Liljebäck (M'08) received the MSc degree from the Department of Engineering Cybernetics, Norwegian University of Science and Technology (NTNU), Trondheim, Norway, in 2004. He is currently a PhD candidate at this department at NTNU, and simultaneously works as a research scientist at SINTEF ICT, Department of Applied Cybernetics, Trondheim, Norway, which is a Norwegian research organization. His research interests include modelling and control of dynamical systems, and design and implementation of mechatronic systems.

Idar U. Haugstuen received the MSc degree from the Department of Engineering Cybernetics, Norwegian University of Science and Technology (NTNU), Trondheim, Norway, in 2010. He recently completed his Master's thesis on control and stability analysis of snake robot locomotion. His research interests include control systems in general and control of mechanical systems in particular.

Kristin Y. Pettersen (S'93–M'98–SM'04) received her MSc and PhD degree in Electrical Engineering at the Norwegian University of Science and Technology (NTNU), Trondheim, Norway, in 1992 and 1996 respectively. In 1996 she became Associate Professor, and in 2002 Professor, at the Department of Engineering Cybernetics, NTNU. In 1999 she was a Visiting Fellow at the Department of Mechanical and Aerospace Engineering, Princeton University, Princeton, NJ and in 2008 Visiting Professor at Section for Automation and Control, University of Aalborg, Denmark. She has published more than 100 conference and journal papers. In 2006 she received the IEEE Transactions on Control Systems Technology Outstanding Paper Award. She is a senior member of IEEE and Associate Editor of the IEEE Transactions on Control Systems Technology. She furthermore holds several board positions in industrial and research companies. Her research interests include nonlinear control of mechanical systems with applications to robotics, satellites, AUVs and ships.